A Study of Elastic Plastic Deformation of Heavily Deformed Spherical Surfaces

by

Saurabh Sunil Wadwalkar

A thesis submitted to the Graduate Faculty of
Auburn University
in partial fulfillment of the
requirements for the Degree of
Master of Science

Auburn, Alabama
December 18, 2009

Keywords: heavy loading, plastic deformation, compression of spheres

Approved by

Robert L Jackson, Chair, Associate Professor of Mechanical Engineering
Jeffrey Suhling, Quina Distinguished Professor, Mechanical Engineering
Pradeep Lall, Thomas Walter Professor of Mechanical Engineering
Lewis Payton, Associate Research Professor of Mechanical Engineering

Abstract

This work uses a finite element analysis and analytical equations to model elastic-plastic and fully plastic large deformations of spheres in contact with rigid flat surfaces. The case considered here is of a deformable sphere compressed by a rigid flat as opposed to the reverse case of a rigid spherical indenter penetrating a deformable surface. Most previous work only deals with elastic or elasto-plastic deformation at much smaller deformations. Based on an extensive literature survey, the work most related to plastic deformations of spherical surfaces are the papers by Noyan [1] and Chaudhri [2]. Even existing finite element based models do not explain plastic deformations well. The current work theoretically explains the initiation and progression of plastic deformations throughout the sphere.

A model for predicting contact area, pressure and force for plastic deformations has been proposed based on the FEM simulations and analytical equations derived from volume conservation. The analytical volume conservation approach is similar to that used to model the barreling of compressed cylinders. The most important aspect of the model is the resulting equation relating the average pressure during fully plastic deformation to the yield strength. The model improves the current state-of-the art by providing equations relating contact force, area, pressure and interference much further into the fully plastic regime and for much larger deformations than the previous works. The results have been compared with existing models and with experimental data. All the results have been

simulated for three different sets of material properties to provide a model that is applicable to a wide range of materials.

Acknowledgments

I wish to acknowledge my sincere gratitude to my advisor, Dr. Robert L Jackson, for his great motivation, support and encouragement during the course of this study. I would like to thank my committee members, Dr. Lewis Payton, Dr.Jeffrey Suhling and Dr. Pradeep Lall, for their continuous support in this study.

I would like to express deep gratitude and gratefulness to my parents and brother for their enduring love, immense moral support and encouragement in my life. I wish to thank all my colleagues and friends at Auburn for their friendship and help.

Table of Contents

List of Figures

List of Tables

Nomenclature

$\overline{A}$	individual asperity contact area
$\overline{A}_n$	nominal contact area
$\left(\frac{a}{R}\right)_{JG}$	ratio of contact radius to original radius predicted by Jackson and Green
$\left(\frac{a}{R}\right)_{new}$	ratio of contact radius to original radius predicted by current study
A_1, A_2	constants based on material properties for deformable base case
A_3, A_4	constants based on material properties for rigid base case
A_c	critical contact area at onset of plastic deformation
A_P	area of contact during plastic deformation
$\overline{A}_{CEB}$	area of contact during elastic-plastic range given by CEB model
$\overline{A}_{KE}$	contact area given by KE model
a	radius of area of contact
B	material dependent exponent
C	critical yield stress coefficient
d	separation of mean asperity heights
E	modulus of elasticity
E'	equivalent modulus of elasticity for the bodies in contact

F	contact force
F_c	critical contact force
F_p	contact force during fully plastic deformation
H	contact pressure during fully plastic deformation or hardness
K	hardness factor
P	contact pressure
$\overline{P}_{CEB}$	contact force during elastic-plastic range given by CEB model
$\overline{P}_{KE}$	contact force given by KE model
R_1	radius of curvature for deformed hemisphere
R_2	radius of curvature for bulged portion of hemisphere
R	undeformed radius of the hemisphere
S_y	yield strength
V_1	initial volume of hemisphere before deformation
V_2	volume of deformed geometry
z	height of asperity measured from mean of asperity heights
(z)	Gaussian distribution
ω	interference between hemisphere and flat rigid surface
ω_c	critical interference between hemisphere and flat rigid surface
δ	barreling constant
υ	Poisson's ratio

CHAPTER 1
INTRODUCTION

Flattening of spherical surfaces in contact with flat rigid surfaces is a problem which has always received a great deal of attention, especially in regards to bearings, tribological surfaces, impacting objects, and thermal and electrical contact resistance. Whenever a sphere is being compressed by a flat surface, it can be classified by different phases of deformation viz. elastic, elasto plastic and fully plastic deformations. Bodies undergoing elastic deformation can recover their original shape but if there is plastic deformation the sphere will get permanently deformed.

To be able to evaluate the behavior of spheres in the elasto plastic and fully plastic regimes one needs to understand the basic elastic-plastic deformations. The stress strain relationship for a body under compression is shown in Fig. (1.1). As shown in the Fig. (1.1), stress increases linearly with strain during small deformations as defined by Hooke's law. However, as deformations get larger, the relationship between stress and strain is no longer linear. Point 'A' is defined as the proportionality limit and upto this point the curve follows Hooke's law. The slope of the line till the proportionality limit is called the Young's modulus of elasticity. As more and more material starts deforming, plastic deformations grow and the curve departs from linearity. As permanent deformations increase, the material becomes saturated with dislocations which prevent nucleation of new dislocations. This is manifested in the form of increased resistance to

deformation and is called work hardening of the material. Materials are many times purposefully work hardened to increase their strength and resistance against plastic deformations by techniques such as cold rolling and cold drawing. The rate of work hardening is defined by the tangent modulus of the stress strain curve beyond the proportionality limit.

Although the theory of elasticity has been studied in detail and ample material is available, work related to understanding and explanation of plastic deformation of spherical surfaces is relatively scarce. Existing models [3], [4], [5], [6] and [7] explain elastic and elasto plastic deformations and predict the contact pressure and contact area to much accuracy and rely on the truncation method for explaining fully plastic deformations. The truncation method proposed by Abbott and Firestone [8] states that under fully plastic conditions the contact area of an asperity in contact with a flat rigid can be calculated by truncating the asperity tips as the flat rigid translates an interference, ω. The details of this model will be discussed later in the literature survey chapter. The limitations in using this approach will be explained in the following sections.

Flattening of a sphere occurs when it is compressed by a rigid surface. As mentioned above, several studies related to this problem have been published. Some of them discussed in the literature review (see chapter 3) are Chang et al. [5], Kogut et al. [9], Jackson and Green [3] and Zhao et al. [10]. These studies discuss elastic and elasto plastic deformations in detail but lack explanation when the contact area becomes larger. The present work investigates this flattening problem for spherical surfaces and proposes a model to better explain the evolution and progression of deformation during elastic, elasto plastic and fully plastic regimes.

Jackson and Green [3] defined a elasto plastic model to address the flattening problem. They defined a limit for the average contact pressure which is valid upto a/R =0.41, where a is the contact radius and R is the original radius. According to them above this value, the deformations become large and the model is not intended for such large deformations. The current study makes an attempt to extend the Jackson and Green model and make it applicable to the plastic deformations and validate it till a/R =1. Initially, the sphere under compressive load has been simulated and analyzed without any strain hardening and friction. However, some results to understand the effects of strain hardening and friction have been discussed later. To validate the FEM based model the results have been compared with existing experimental data [2]. The following section explains the motivation and objective of the research work. Based upon the research and comparisons with existing real world data, results will be presented and conclusions will be made.

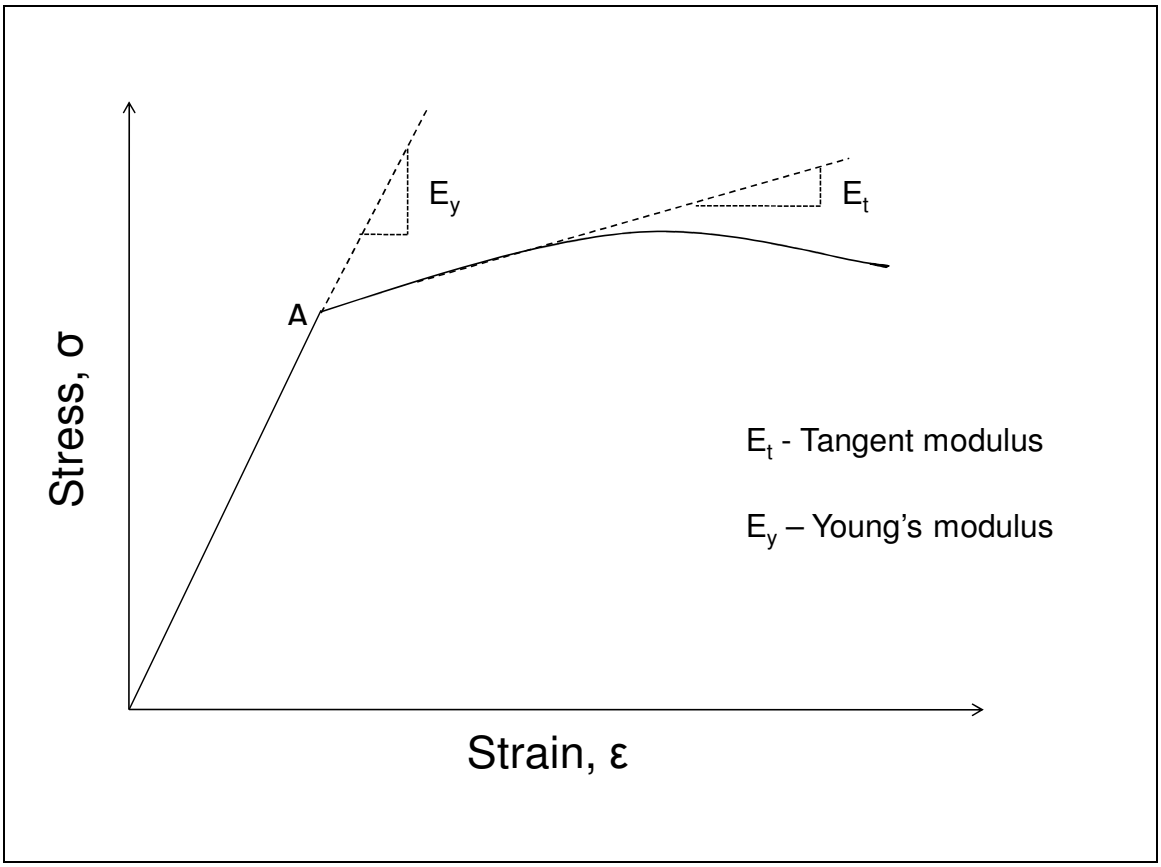

Figure 1.1: Stress strain curve for a sphere under compression

CHAPTER 2

MOTIVATION AND OBJECTIVES

Motivation:

Two primary motivating factors for the present investigation on flattening of spheres by rigid flat surfaces are

1) Better understand evolution and progress of plastic deformation during flattening of spherical surfaces. Existing models poorly predict contact parameters such as contact force and area for large deformations.
2) For heavily loaded spherical contact, the effects of strain hardening have scarcely been documented. It is important to understand this hardening effect in the sphere under compression.
3) Existing models (see literature survey) do not compare results with real world experimental data for heavily loaded spherical surfaces. A theoretical description of compression of spherical surfaces under heavy loading in the fully plastic regime is not available.

Objectives:

Based on these above factors, the chief objectives of the current investigation are defined as to

1) Provide a comprehensive technical literature review on the flattening problem of spherical surfaces.
2) Propose a finite element based model which explains and predicts the deformation behavior of heavily loaded spheres.
3) Present and discuss the effects of strain hardening and friction in the current study.

CHAPTER 3

LITERATURE REVIEW

The problem of compression of spherical surfaces by flat surfaces has received great attention and a significant amount of work has been published related to this problem. When a sphere is compressed between flat surfaces, the sphere undergoes different phases of deformation before complete failure. For low loads, the deformation is mostly elastic. But as loads get larger, permanent deformation is observed which results in plastic deformation. Once the sphere load passes a critical value, at a point below the surface the Von Mises stress exceeds the yield strength and plastic deformation begins. The fully plastic regime is defined as when the entire contact area is deforming plastically.

Most previous spherical contact models consider the elastic or elastic-plastic case, but do not study the fully plastic regime in depth [5], [9] and [3]. Chaudhri et al. [2] and Noyan at al. [1] have conducted experimental analysis of spherical contact in the fully plastic regime, but no theoretical studies appear to have been conducted for the flattening case. There is a great deal of work which also considers indentation in the elastic, elasto-plastic and fully plastic regime [3], [11], [7] and [12]. Indentation means that the sphere is rigid and the flat surface deforms. However, the current work is concerned only with flattening rather than indentation. In flattening, the flat surface is

rigid and the sphere is deformable. Whenever a metal sphere is compressed between flat rigid surfaces, it undergoes elastic, elasto plastic and fully plastic deformation. In this work we refer to this case as flattening. Jackson and Kogut [11] also compared these two cases and showed how their behaviors are very different. This configuration is relevant in many other areas such as forging and anisotropic conductive films [13], [14], [15] and [16]. The following sections are aimed to give a summary of the literature that is available related to flattening of spherical surfaces.

Experimental work – Plastic compression of spheres

Two of the most noteworthy previous works on spherical flattening in the fully plastic regime are the experiments conducted by Chaudhri et al. [2] and Noyan [1]. Chaudhri et al. [2] conducted experiments to characterize the behavior of spheres made of different materials and with different prior treatments (work hardened or annealed). The different materials used for the experiments were phosphor bronze (92% Cu, 8% Sn), brass (60% Cu and 40% Zn) and aluminum. The experimental setup used by Chaudhri et al. [2] included two different flat surfaces for compression at high and low loads. For low loads, the spheres were compressed between sapphire plates backed by a glass plate which rested on a strong metal support. A calibrated graticule in the viewing microscope measured the diameter of contact area. For high loads (plastic deformation) the sphere was compressed between polished plane tool-steel platens at a cross head speed of 5 mm min^{-1} in a J.J modeled T5000 testing machine. The diameter of the area of contact was measured by an optical microscope after unloading. A detailed discussion of the evolution and progress of deformation is presented. The effects of lubrication on fully

plastic contact have also been studied. The current work uses this experimental data to compare to and validate the FEM results.

In Chaudhri et al. [2] the spheres, both undeformed and compressed were sectioned and measured for microhardness across the diameter of the sections using a Leitz miniload hardness tester. Care was taken so that the indentations do not interfere with each other. The hardness measurements for the as-received phosphor bronze before and after loading revealed that there was hardly any hardening left in the material. Thus, these can be treated as elastic perfectly plastic materials in the experiments. The current work models the sphere as elastic perfectly plastic initially and will use the experimental results to validate the simulation results.

The experimental work by Noyan [1] focused mostly on compression of solid spheres of various materials between parallel platens. During the experiments, the variation in contact area and area of the central plane of symmetry with plastic deformation was monitored. They defined two normalized parameters which are independent of size and material of the sphere. This indicated that according to them, plastic deformation of spheres was controlled by geometry. They also mapped the microhardness throughout the sphere and predicted the distribution of deformation. Some of the conclusions of these experiments are:

- An increase in contact area is a function of the depth of penetration of the flat rigid surface
- The hardness distribution in the deformed spheres is symmetric across the central plane

- As the compressive strain increases, the plastic deformation progresses deeper into the sphere.

The current work will confirm these findings with analysis of finite element modeling results for spheres without any strain hardening. But an attempt to understand strain hardening effects during compression will also be made later.

Fully plastic contact models

Tabor [17] studied the contact between a sphere and a flat surface under compression loads. He showed from slip-line theory that the hardness of a perfectly plastic spherical indentation should be about

$$H = 2.8 \cdot S_y \tag{1}$$

The hardness, *H*, here is defined as the average pressure during fully plastic contact or indentation. These formulations are empirical and have been defined for a variety of materials like aluminum, copper and mild steel. According to Tabor [17], the relationship between mean pressure and the yield stress changes from $P = 1.1 \cdot S_y$ to $H = 2.8 \cdot S_y$ during the transition from elasto plastic to fully plastic deformations. Notice, the pressure is addressed by *P* and *H*. For fully plastic deformations, the mean contact pressure (hardness) is also denoted by *H*. These relationships are derived from frictionless compression experiments.

Although often attributed to the earlier work by Abbot and Firestone [8] but probably actually derived by Greenwood and Tripp) [18], a model for contact area of a fully plastic spherical contact was created by simply truncating the sphere geometry with the flat surface. Then the contact area can be approximately calculated by truncating the sphere tip as it translates an interference, ω, without deformation into the flat surface. For a hemisphere, this approximated fully plastic contact area is be given by

$$A_P = 2\pi R\omega \tag{2}$$

The contact force is then just Eq. (2) multiplied by the contact pressure which in this case is the hardness, since the contact is assumed to be fully plastic and is given by,

$$F_p = 2\pi R\omega H \tag{3}$$

Eq. (3) has been proven erroneous by many works [3], [7] and [11] for both the indentation and flattening cases. This is because it is overly simplistic and neglects the actual elastic-plastic contact mechanics that take place during contact. The major criticism in addition to this is that it does not conserve the volume of the material deforming plastically.

Ishlinsky [31] also proved analytically by using the Harr-Karman criterion of plasticity that it is possible to determine the mean pressure for spherical contact. According to Islinsky [31] the value of the constant in the relation between the mean

contact pressure and the yield strength is 2.84. This value of the constant was confirmed by Johnson [32] who mention a value of 2.84 for the constant in their work. Whereas, Ashby [33] reported that the value of constant in their study was found to be 3.3. This discrepancy in the value of this constant was studied in detail and a range of 2.8 to 3.3 was observed to be reported in various texts referred to in the current study.

Elastic and Elasto plastic models

Chang et al. [5] developed a plastic contact model (CEB) that supplemented with the GW model explained later. The GW model is an elastic contact model. CEB model used the volume conservation principle similar to the current study to approximate a elastic-plastic contact. Assumptions of the CEB model are,

- A fixed relationship between yield strength and hardness, $H = 2.84S_{y.}$
- The hemisphere behaves elastically below the critical interference ω_c and fully plastically above it.
- Deformation is localized near the hemisphere's tip.

According to the CEB model, the contact area and force for $\omega/\omega_c > 1$, that is the elastic-plastic range are given by

$$\overline{A}_{CEB} = \pi R(2\omega - \omega_c) \tag{4}$$

$$\overline{P}_{CEB} = \pi R(2\omega - \omega_c)KH) \tag{5}$$

where,

$$\omega_c = \left(\frac{\pi K H}{2E'}\right)^2 R \quad \text{and} \quad K = 0.454 + 0.41\upsilon$$

The limitations of the CEB model are that it assumes the fixed relationship between hardness and yield strength. This assumption was proved incorrect by Jackson and Green [3]. Also, the model has discontinuity at ω_c.

Kogut and Etsion [9] performed an FEM analysis for the flattening case of sphere in contact with a flat rigid surface. Their work gives a very detail stress distribution study in the contact area. The contact force and area are defined for ranges of ω/ω_c.

For $1 \leq \omega/\omega_c \leq 6$,

$$\overline{P}_{KE} = \overline{P}_c 1.03\omega/\omega_c^{1.425} \tag{6}$$

$$\overline{A}_{KE} = \overline{A}_c 0.93\omega/\omega_c^{1.136} \tag{7}$$

For $6 \leq \omega/\omega_c \leq 110$,

$$\overline{P}_{KE} = \overline{P}_c 1.40\omega/\omega_c 1.263 \tag{8}$$

$$\overline{A}_{KE} = \overline{A}_c 0.94\omega/\omega_c^{1.146} \tag{9}$$

The KE model similar to the CEB model assumes a fixed relationship between hardness and yield strength $H = 2.84S_y$. Also, the model equations are discontinuous at $\omega/\omega_c = 1$ and 6. KE model only describes deformations till $\omega/\omega_c = 110$. Beyond this point the truncation model [8] is assumed to define the fully plastic deformations.

Zhao et al. [10] worked on a elasto-plastic asperity microcontact model for rough surfaces in contact. The model incorporates the transitional regime from elastic to fully plastic deformations. The model like the CEB [5] and KE [9] models assumes truncation model for fully plastic deformations. Nuri [19] reported rough surface contact parameters by experimentally measuring them. Jackson and Green [4] compared their predictions of contact radius to show that the bulk material below the asperities would undergo extreme deformation. [20] gave analytical approximations for modeling rough surface contacts. Jackson and Green [3] find that Eq. (3) can overpredict the contact force. They propose a FEM based elasto-plastic contact model for the contact between a deformable sphere and a flat rigid surface. Their work finds that the hardness or the fully plastic average contact pressure actually varies with the deforming geometry of the sphere. Chaudri et al. [2] also confirmed this experimentally. When the contact pressure is plotted against the contact radius, a limit appears to emerge for the average pressure during fully plastic contact. According to Jackson and Green [3], as a/R increases, the limiting average pressure to yield strength ratio must change from Tabor's [17] predicted value of approximately 2.84 to a theoretical value of 1 when $a=R$. This has been depicted in the Fig. (3.1).

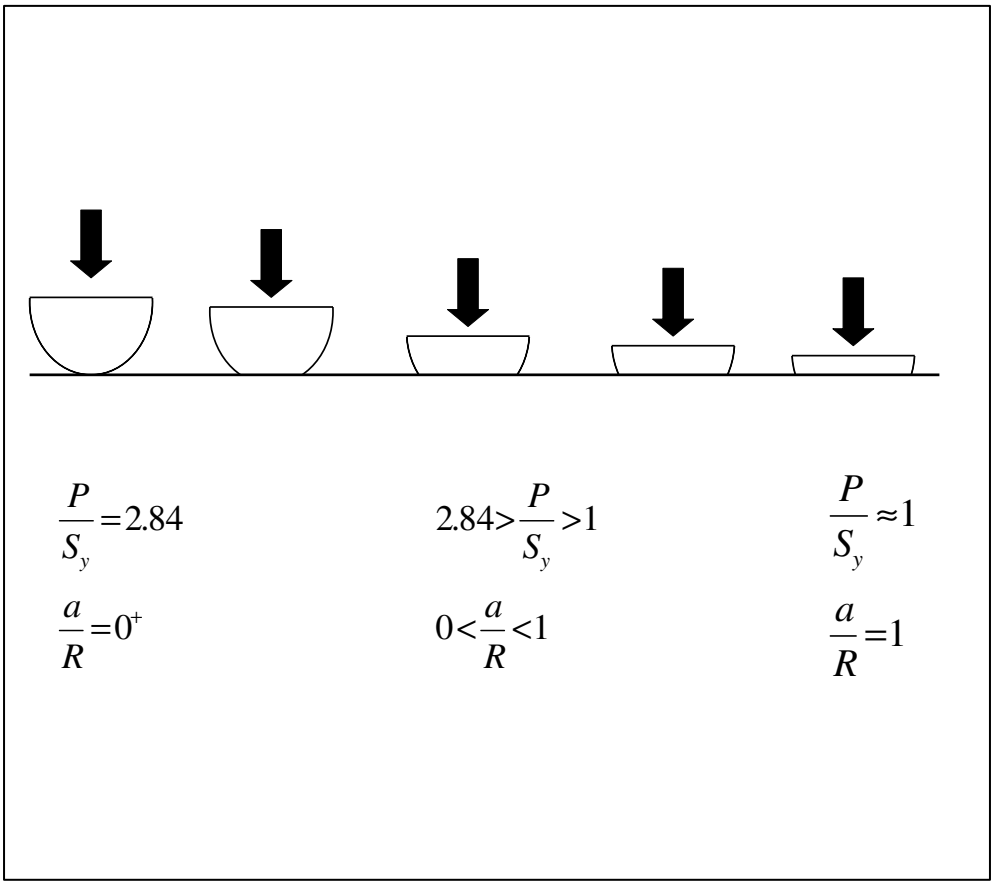

Figure 3.1: Figure showing the assumption by Jackson and Green.

As the interference increases the contact geometry changes and when the contact radius $a=R$, the geometry is similar a cylinder in contact with a flat rigid surface. For the case of the cylinder in compression, the value of P/S_y is theoretically equal to 1.

By fitting a function to their FEM results, Jackson and Green [3] provide the following formula:

$$\frac{P}{S_y} = 2.84\left[1-\exp\left(-0.82\left(\frac{a}{R}\right)^{-0.7}\right)\right] \tag{10}$$

Note that in Eq. (10) P is used instead of H as the symbol for the average pressure during elasto-plastic contact. This is used here to emphasize that the P predicted by Eq. (10) varies with the deformation of the sphere, whereas the traditional value of H does not. The FEM based model also provides predictions of the contact force during elastic-plastic contact as,

$$\frac{F}{F_c} = \left[\exp\left(-\frac{1}{4}\left(\frac{\omega}{\omega_c} \right)^{\frac{5}{12}} \right) \right] \left(\frac{\omega}{\omega_c} \right)^{\frac{3}{2}} + \frac{4P}{CS_y} \left[1 - \exp\left(-\frac{1}{25}\left(\frac{\omega}{\omega_c} \right)^{\frac{5}{9}} \right) \right] \frac{\omega}{\omega_c} \tag{11}$$

where,

$$C = 1.295 \exp(0.736\upsilon)$$

The ratio of pressure to the yield strength in Eq. (11) is calculated using Eq. (10). Quicksall et.al [21] also verified these results for a wider range of material properties by varying E (Young's modulus) and S_y (Yield Strength).

In another study, Jackson and Green [4] related the contact radius of the sphere to the interference ω, of the flat rigid surface into the sphere. They worked on predictions of the contact radius during elastic and elastic- plastic contact. Jackson and Green [4] predicted the ratio of contact radius to the original radius as

$$\frac{a}{R} = \sqrt{\frac{\omega}{R}} \left(\frac{\omega}{1.9\omega_c} \right)^{B/2} \tag{12}$$

where,

$$B = 0.14 \exp\left(23 \left(\frac{S_y}{E'} \right) \right)$$

Due to the limited range of FEM cases used to find Eq. (12), these models are only valid for normalized contact radii of $0<a/R\leq 0.412$. The underlying assumption of the Jackson and Green study is that the nominal radius of the sphere under compression remains constant. For large deformation like in the current study, the radius of the sphere can either bulge outward or the area of the central plane of the sphere will increase.

Jackson, Marghitu and Green (JMG) [22] presented a study about numerically predicting the coefficient of restitution for impacting spheres. The spheres were considered to show elastic perfectly plastic behavior. The work uses finite element analysis results for static deformation of spheres from Jackson and Green (JG) [3] and equations of variation of kinetic energy to predict the coefficient of restitution. The JMG [22] model provided a more concise version of the equation for the ratio of limiting contact pressure to the yield strength than provided by the JG model. This equation was also intended to increase the range of validity to $0<a/R\leq 1$ but is unconfirmed. It accomplished this by finding an equation that fit the JG model where $a/R\leq 0.412$ but also when $a/R = 1$, $P/Sy = 1$

$$\frac{P}{S_y} = 2.84 - 0.92\left[1 - \cos\left(\pi \frac{a}{R} \right) \right] \tag{13}$$

Like the JG model, this elastic perfectly plastic model assumes that the radius of the sphere will remain constant during deformation which is not the case for heavy loading as in the current study. The current study uses the above equation and modifies it to predict the ratio of this limiting average pressure to the yield strength.

Most recently, Megalingam and Mayuram (MM) [23] created a FEM based model for predicting contact area and contact force as a function of interference. The model mainly compares its results with the Greenwood Williamson model (statistical model) [18] for contact load and area. The model is meant for simulating asperity contact. The results of a deterministic model are validated by developing a statistical model, in which the asperities are modeled as hemispherical in shape and without interaction with the neighboring asperities (Greenwood Williamson statistical model assumptions).

According to the model by MM, the area of contact and contact load for various phases of deformation can be calculated using a set of equations given below. The various phases of deformation viz. elastic, elasto plastic and fully plastic are addressed by increasing values of the ratio of the interference to the critical interference.

According to this model, for $\omega/\omega_c \leq 1.05$, only elastic deformation needs to be considered because the volume of the plastically deforming material is very small. Above this value, the contact area and load can be predicted using Eq. (14) and (15),

$$\left.\begin{array}{ll} 1.05 < \dfrac{\omega}{\omega_c} < 80, & \dfrac{A}{A_c} = 1.0733\left(\dfrac{\omega}{\omega_c}\right)^{1.1169} \\ 80 < \dfrac{\omega}{\omega_c} < 150 & \dfrac{A}{A_c} = 2.5067\left(\dfrac{\omega}{\omega_c}\right)^{0.9221} \\ 150 < \dfrac{\omega}{\omega_c} < \infty, & \dfrac{A}{A_c} = 6.1966\left(\dfrac{\omega}{\omega_c}\right)^{0.7399} \end{array}\right\} \quad (14)$$

$$\left.\begin{array}{ll} 1.05 < \dfrac{\omega}{\omega_c} < 10, & \dfrac{F}{F_c} = 1.0392\left(\dfrac{\omega}{\omega_c}\right)^{1.4111} \\ 10 < \dfrac{\omega}{\omega_c} < 80, & \dfrac{F}{F_c} = 1.7035\left(\dfrac{\omega}{\omega_c}\right)^{1.202} \\ 80 < \dfrac{\omega}{\omega_c} < 150, & \dfrac{F}{F_c} = 8.1242\left(\dfrac{\omega}{\omega_c}\right)^{0.8402} \\ 150 < \dfrac{\omega}{\omega_c} < \infty, & \dfrac{F}{F_c} = 46.165\left(\dfrac{\omega}{\omega_c}\right)^{0.4873} \end{array}\right\} \quad (15)$$

where Eq. (14) and (15) in [23] are claimed to be valid until infinity. The results of the current work will be compared to the equations mentioned above (see Eqs. (14 and 15)).

Shankar and Mayuram (SM) [24] worked on the same problem. In the SM model, a single asperity contact is considered based on elastic perfectly plastic contact to an infinite non dimensional interference. The empirical relationships proposed by this model

are of a similar nature to the Malingam Mayuram model but are valid only till a range of $\frac{\omega}{\omega_c} < 450$.

Statistical model

The contact models proposed in the previous sections can be used to model the contact of single bumps or asperities on the rough surfaces in contact. Greenwood and Williamson (GW) [18] in their work modeled rough surfaces as a set of independent asperities of constant radius and variable height depending on the height distribution function. According to the model, the nominal area of contact and contact load can be calculated using,

$$A(d) = \eta A_n \int_d^\infty \overline{A}(z-d)\phi(z)dz \tag{16}$$

$$P(d) = \eta A_n \int_d^\infty \overline{P}(z-d)\phi(z)dz \tag{17}$$

where, A_n is the nominal or apparent area of contact and $\overline{A}$, $\overline{P}$ and $\varphi(z)$ are the area of contact, contact load and Gaussian height distribution function for individual asperities. Also, d is the distance between the mean of the summit heights.

The GW model then assumes that all the hemispherical asperities deform elastically and are defined by the Hertz solution [25]. The GW model is relatively simple and has a few shortcomings. The model's dependence of spectral moments on the

resolution of the surface measuring apparatus and sample length renders the accuracy of this model highly dependent on the measuring device. Also, this model assumes a constant radius of curvature for all the asperities. The original GW paper is for perfectly elastic contact. Later researchers tried to improve it by including elastic plastic asperity models [4], [5] and [9]. The current study is for plastic deformations of spheres and the radius of the sphere will constantly change at every load step because of the heavy loading.

As discussed previously, lightly loaded spherical contacts in the elastic and elastic-plastic regimes have been given more attention in comparison to those heavily loaded in the fully plastic regime and have been explained analytically as well as experimentally. In contrast, work related to higher loads and the fully plastic regime is scarce. By using finite element analysis tools and volume conservation theory, an attempt to study fully plastic contact has been made. The analysis has also resulted in a new model for spherical contact that appears to be valid over a much larger range than any previous model. The model helps in predicting the contact area, pressure and force during heavily deformed contacts to a much greater accuracy than previous models. Even though the model assumes frictionless contact and no hardening, it compares fairly well with the experimental data from Chaudhri [2] and Noyan [1].

CHAPTER 4
FINITE ELEMENT MODELING METHODOLOGY

Introduction

This chapter describes in detail the methodology used to build the finite element model. Two different models are built based on the boundary conditions across the sphere base (explained in detail later in this chapter). The two cases are called

1) Deformable base case
2) Rigid base case

The cases have been classified depending on whether the base is allowed to deform in the X-direction or not. Fig. (4.2) depicts the boundary conditions across the spherical surface. The sphere has been initially modeled as elastic-perfectly plastic but later strain hardening is introduced by varying the tangent modulus of the material.

Boundary conditions

For the simple case of fully plastic spherical flattening contact there are two important cases that have been considered in the current study, namely the 1) deformable base case where the base cross-section of the sphere is able to deform in the radial direction but is held stationary in the direction normal to the base as seen in Fig. (4.1(a)) and the 2) rigid base case where the base is fixed in all directions as shown in Fig.

(4.1(b)). These two cases have been considered because they both are applicable to real situations or problems.

Due to symmetry case 1 is more representative of a sphere being compressed between two parallel surfaces. Since it does not have any resistance perpendicular to the axis of loading, it will deform radially outward in that direction. This case can be compared to deformation of a full sphere. The areas where this case can be considered are anisotropic conductive fills, studies involving flattening of particles. Case 2 might be more realistic for the case of a spherical asperity or bump located on a larger, stiffer surface. Asperity contact, nanodots are some of the examples of the rigid base case.

These cases do not differ significantly for small deformations ($a/R << 1$), but for large deformations these boundary conditions become more significant ($a/R \approx 1$). For lightly loaded contacts the high stresses are isolated mostly to the region near the contact and so the boundary conditions at the base are not important. As the deformation increases and the stresses distribute through the sphere, the boundary conditions will cause the two cases to diverge. This observation follows St. Venant's Principle*.

As a sphere is heavily loaded into the fully plastic regime, the width or diameter at the central plane of the sphere may become larger than the radius of the undeformed original diameter of the sphere (see Fig. 4.3). This is especially true for the case of a sphere with a deformable base (see Fig. 4.3(a)). The increase in the deformed radius effectively decreases the value of a/R used in Eqs. (10 and 13).

** According to the St.Venants principle, "the strains that can be produced in a body by the application, to a small part of its surface, of a system of forces statically equivalent to*

zero force and zero couple, are of negligible magnitude at distances which are large compared with the linear dimensions of the part." [26].

For smaller loads ($a<<R$) the radius will not increase by a great amount but as the loads get larger the change in the radius plays a crucial role in accurate prediction of contact pressure and contact forces, as will be seen in the results. Therefore, it is very important to include this increasing instantaneous radius in any model used to describe plastic deformations. The second case considered is that of a sphere held rigid at its base (Case 2). For the rigid base case, a hemisphere is sitting on a rigidly held base and the base cannot increase in radius as was considered in the deformable base case. However, as the contact radius approaches the size of the fixed base radius, the middle portion of the hemisphere may actually bulge out (see Fig. 4.3(b)). This mechanism is similar to the occurrence of barreling in highly loaded cylinders [27], [28], [29] and [30]. The difficulty is determining the amount of bulging or widening that will occur.

An FEM analysis has been presented to predict the pressure and contact radius between the flat rigid surface and the hemisphere for fully plastic deformations for the deformable and rigid base cases. This contact radius can be substituted in Eq. (13) along with the instantaneous radius calculated using volume conservation principle (see chapter 6) for more accurate predictions of contact pressure.

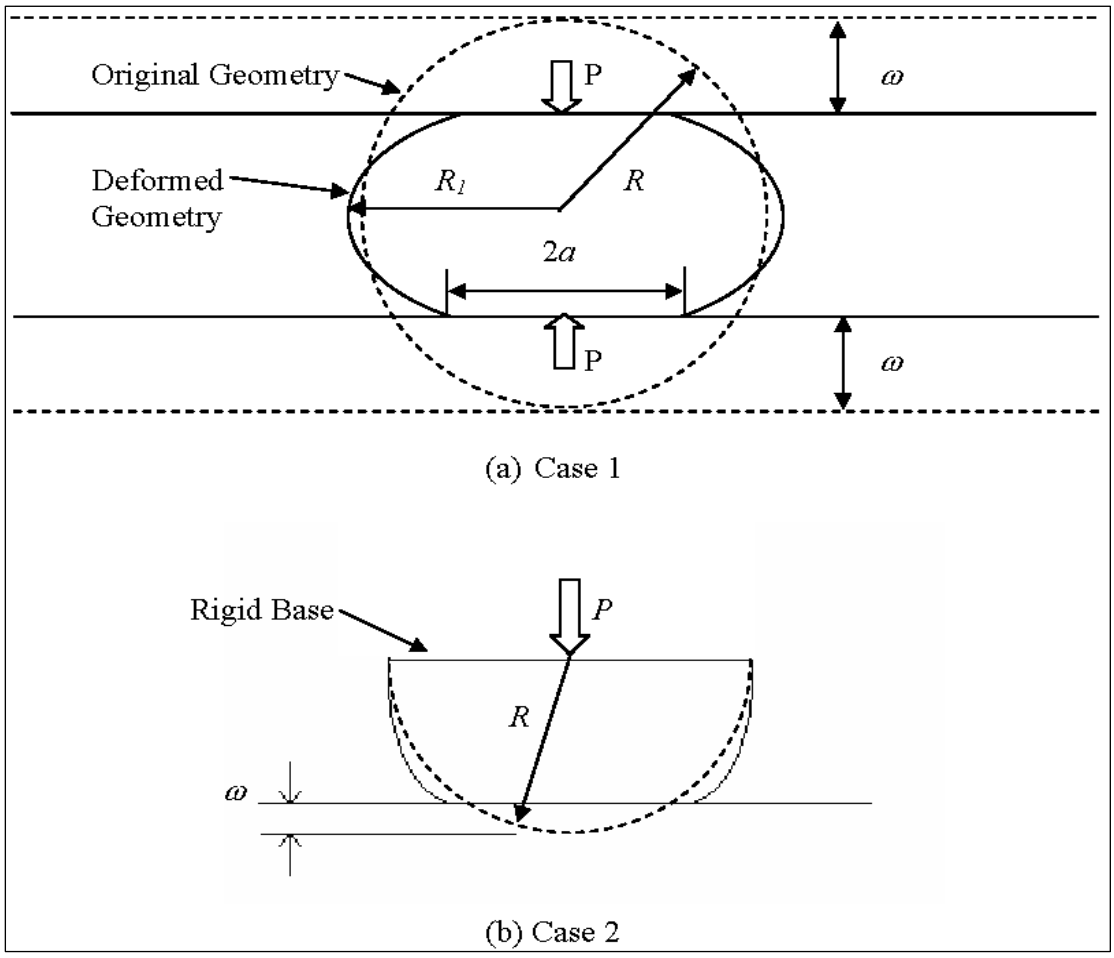

Figure 4.1: The two boundary conditions used to model the sphere

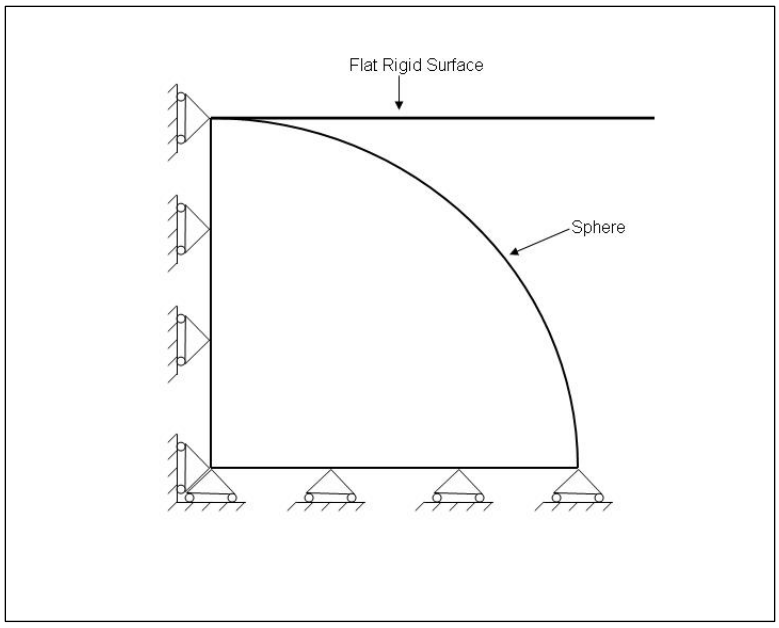

(a) Deformable Base

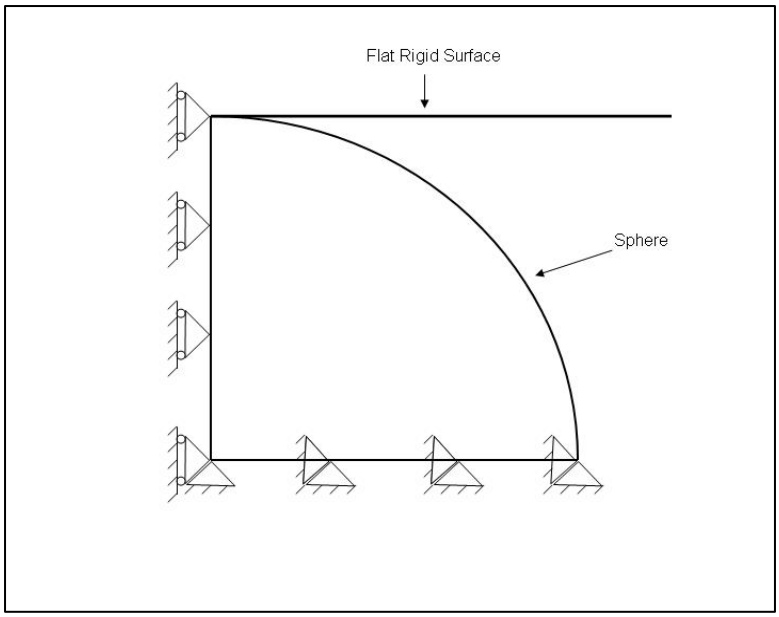

(b) Rigid Base

Figure 4.2: Schematic showing the boundary conditions used n the FEM for the two different cases: *deformable base (case 1)* and *rigid base contact (case 2).*

Simulation Methodology

To analyze the large scale deformation of a sphere loaded against a rigid flat surface, an axisymmetric finite element model has been created using the commercial package Ansys™. The mesh used for solving the problem for the deformable base and rigid base cases are shown in Fig. (4.3a and 4.3b) and have been evaluated by mesh convergence. The original meshing of the undeformed sphere is shown in the appendix in Fig. (A.1). Mesh convergence analysis was performed for maximum displacement across the sphere for the last load step. Five different mesh densities have been used for the mesh convergence analysis. The five meshes consist 86, 321, 706, 1493 and 1926. It has been shown in Figs. (4.4) and (4.5) that the mesh consisting 1493 elements gives accurate predictions of maximum displacement and reaction forces (see Table 4.1) and hence the same is used through out the analysis. The selection criterion for the mesh convergence was less than 0.1% difference between the predictions for increasing number of elements. As can be seen in table 4.1 the error between the predictions of reaction force for increasing number of elements becomes less than 0.1% only when there are 1493 elements. Therefore the maximum displacement and reaction force predictions converge at 1493 elements and hence the same is used in the analysis. Contact between the sphere and the rigid surface is simulated using contact elements (2-D 3nodel contact elements). The elements used in the study are PLANE82 (2-D 8 node element) to model the sphere and CONTA172 and TARGE169 to model the contact between the surfaces. The contact is simulated using Lagrange method in the normal direction and penalty method in the tangential direction of the surface. This is an axisymmetric problem and only a 2-D quarter section of the entire sphere has been modeled. The flat rigid surface has been

modeled as a line and the sphere as a quarter circle. Initially, the problem has been simulated to be a frictionless contact problem and the sphere material has been modeled as elastic-perfectly plastic and without strain hardening. The Von Mises yield criteria has been used to predict the initiation of plastic deformation.

Since for fully plastic deformation the stresses are limited by the yield criteria, the stresses are fairly evenly distributed throughout the sphere when it is heavily loaded. Hence the required mesh density is not as great as that required in a typical FEM analysis of elastic-plastic spherical contact under lower loads. A mesh convergence analysis was also conducted in order to verify the accuracy of the mesh and to save computational time. As the force and the area of contact are the most important parameters to be observed, the same were chosen for this mesh convergence analysis.

To solve the problem, displacements have been applied and contact forces are calculated after the simulation. Another way of solving this problem is by applying force and then calculating the displacements. According to Jackson and Green [3], the first mentioned method is better for rapid convergence. The same method is used in the current study. The penetration or interference between the flat rigid and the sphere, ω, was increased in a stepwise fashion for every time step. Another goal of this study was to show that the results are independent of the material properties and are dependent on the deforming geometry of the sphere. To vary material properties the yield strength values were changed for each simulation. The values used were 1 GPa, 0.5 GPa and 0.2 GPa. The Young's modulus of elasticity was kept constant at 200 GPa.

Strain hardening is an important effect to be considered when studying compression of spheres. The current FEM model uses the Bilinear Isotropic Hardening

(BISO) option to model the nonlinear behavior of the spheres beyond the proportionality limit. This option uses the Von Mises yield criteria with isotropic work hardening assumption. The BISO approach is preferred to model the nonlinearity since this is the option mentioned to be used for large strain analyses according to ANSYS Documentation. Friction will also play a crucial role in the predictions of contact pressure. Results of FEM simulations for effects of increasing values of coefficient of friction across the contact area on the predictions of contact pressure have also been presented. The strain hardening and friction results are preliminary and need more detail study.

(a) Deformable Base

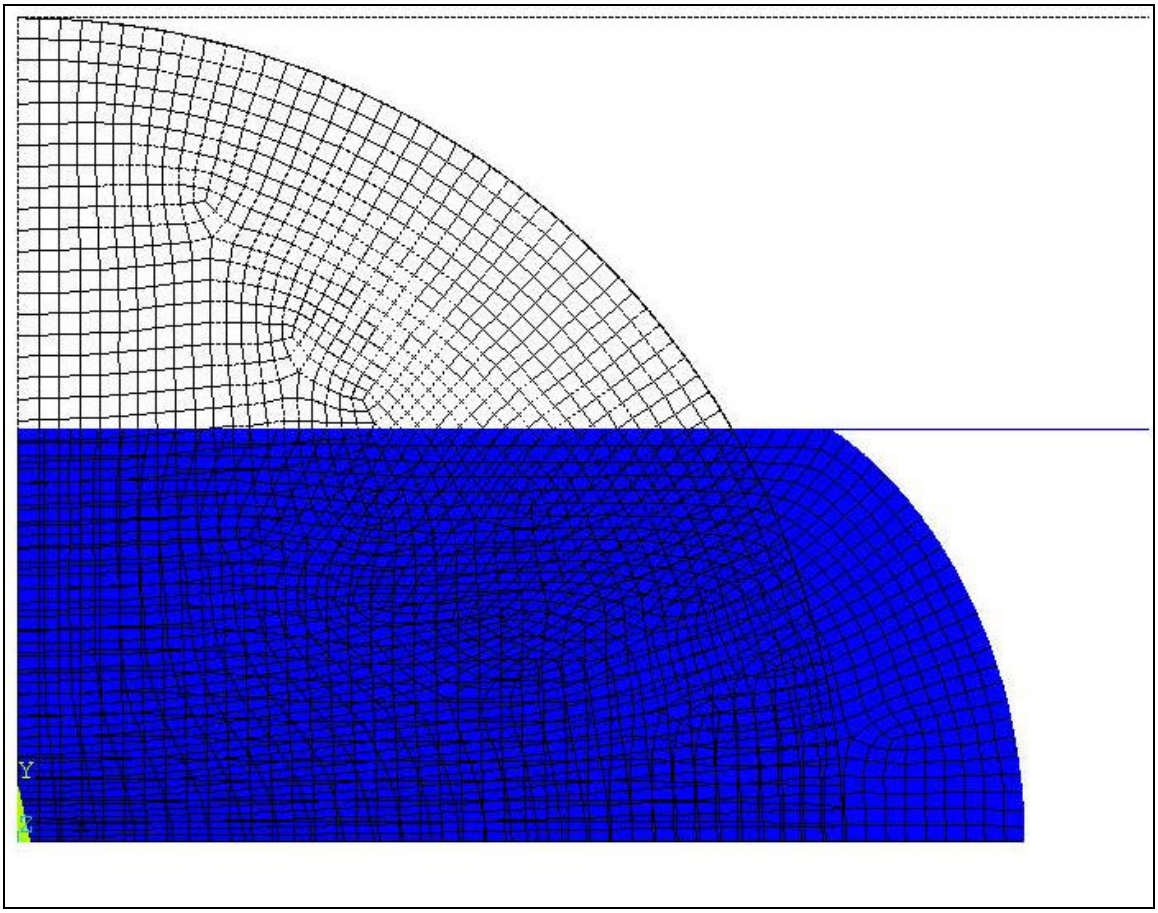

Figure 4.3(a): A representation of the FEM mesh and the deformed geometry of loaded spheres for the deformable base case

(b) Rigid Base

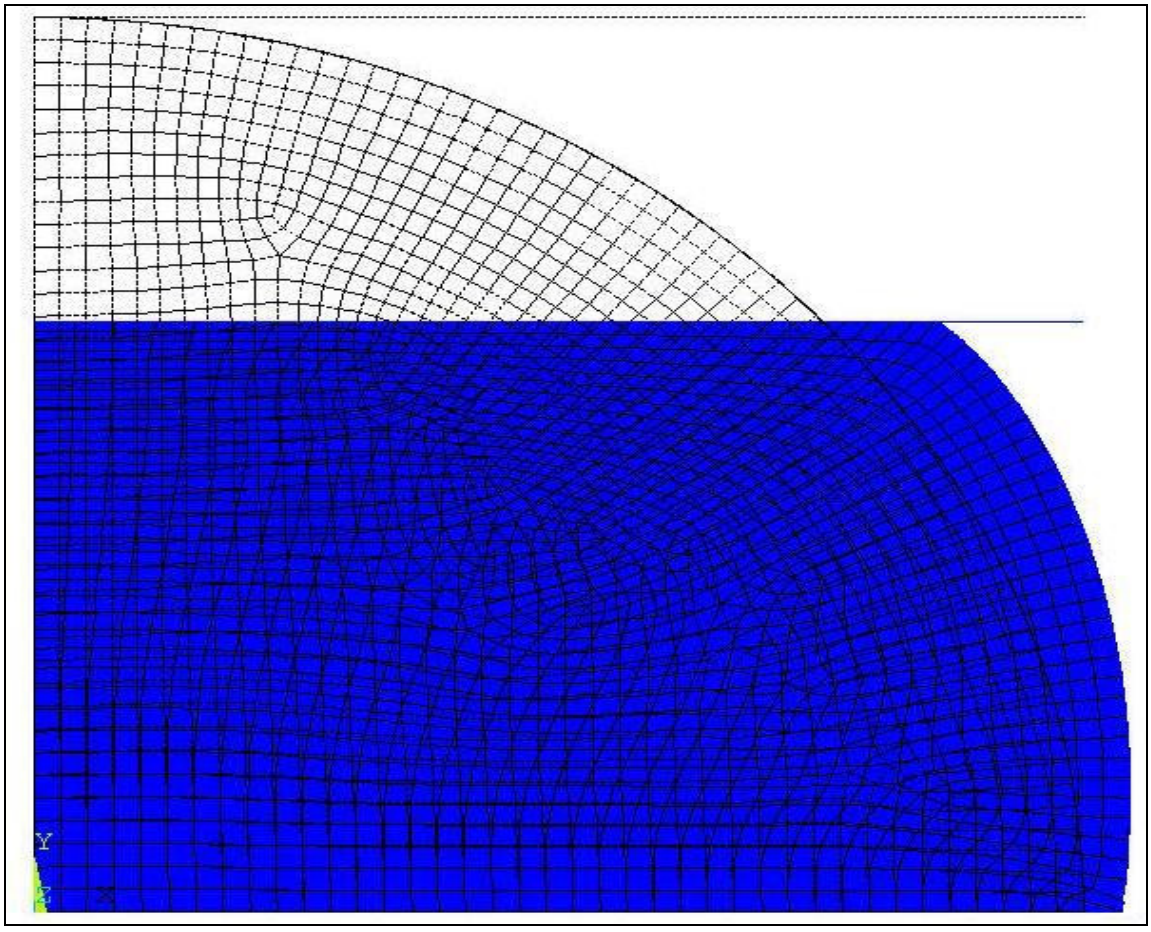

Figure 4.3(b): A representation of the FEM mesh and the deformed geometry of loaded spheres for rigid base case

(a) No.of elements = 86

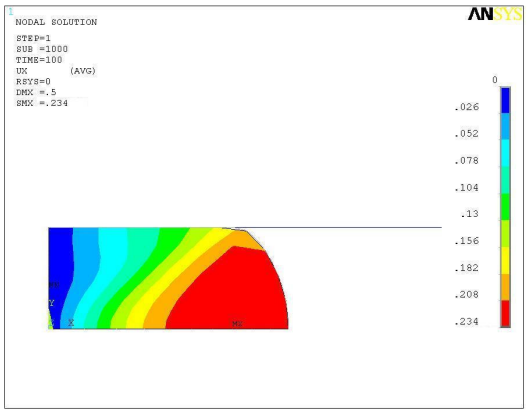

(b) No.of elements = 321

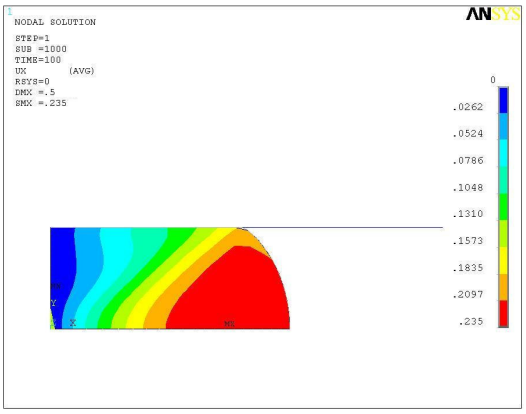

(c) No.of elements = 706

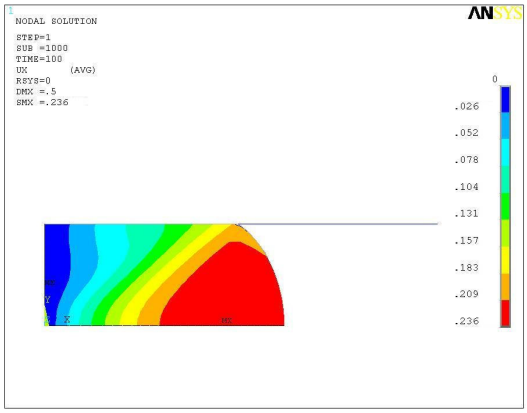

(d) No.of elements = 1493

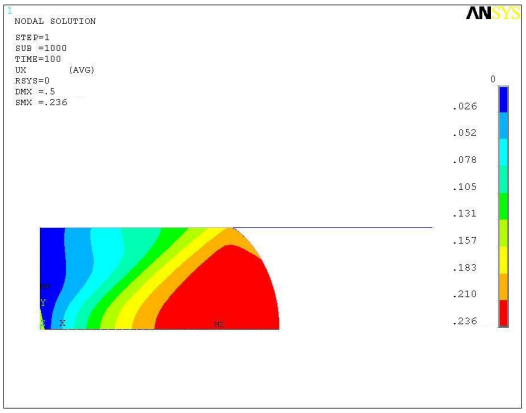

(e) No.of elements = 1926

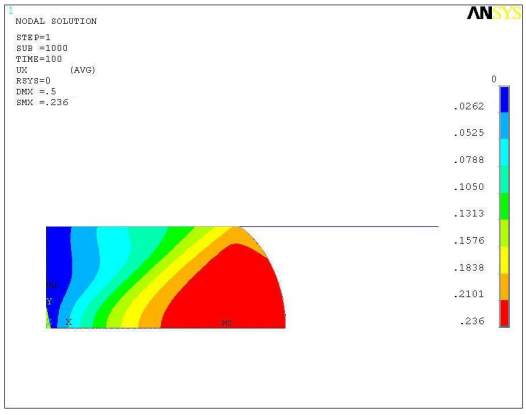

Fig 4.4: Distribution of displacements across the sphere

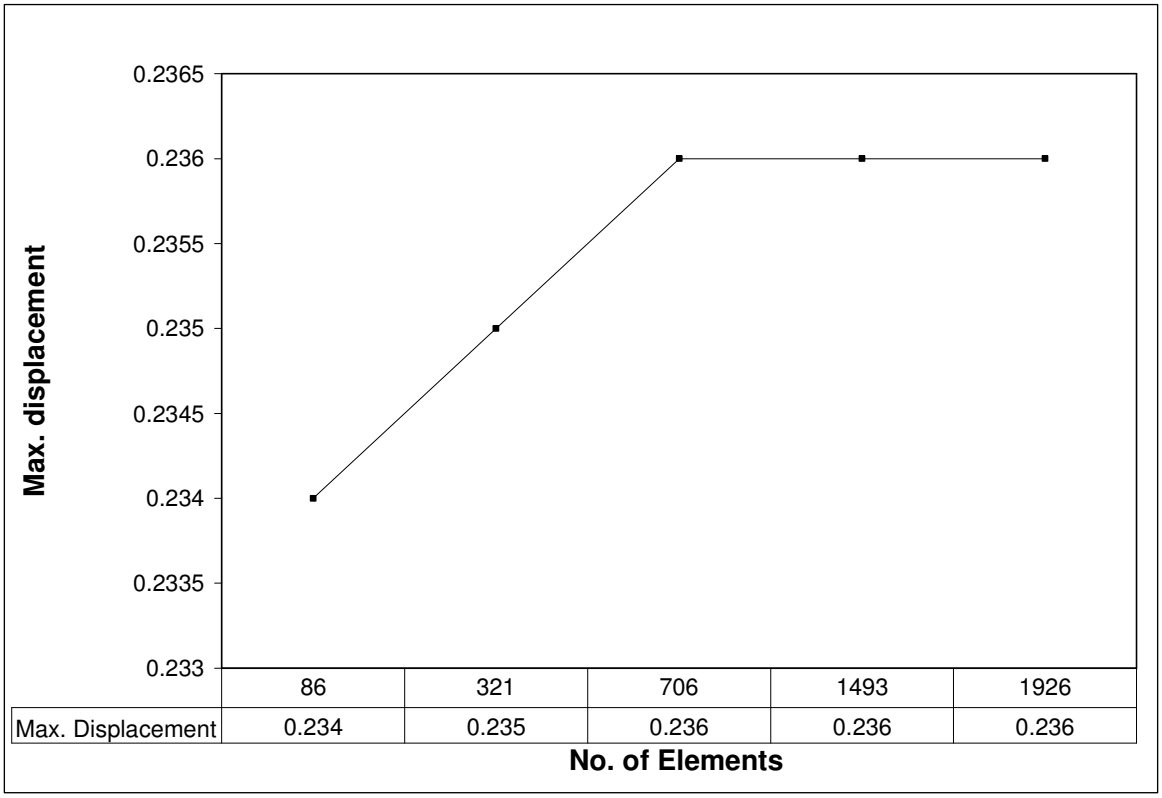

Fig. 4.5: Mesh convergence for maximum displacement across the sphere

Table 4.1: Reaction force results from FEM for mesh convergence

No. of elements	Reaction forces	% Error
86	3.821E+09	
321	3.790E+09	0.817942
706	3.780E+09	0.26455
1493	3.758E+09	0.585418
1926	3.756E+09	0.053248

CHAPTER 5
RESULTS AND DISCUSSION

Introduction

The problem of flattening of a sphere in contact with a flat rigid surface has been modeled in the fashion as explained in the previous chapter and the results are presented in this chapter. The study also aims to study the effects of strain hardening and friction at the area of contact between the sphere and the flat surface. Three different models have been built in order to simulate a sphere 1) with strain hardening 2) without strain hardening and 3) without strain hardening but with friction during compression. A summary of the boundary conditions, strain hardening and friction considerations in the FEM analysis has been presented in table. (5.1). For case 5.1, the model has been simulated to have no strain hardening and no friction during loading. This is elastic perfectly plastic behavior. The model has been built for the two boundary conditions of deformable and rigid base boundary conditions which have been explained in detail in the previous chapter. Case. 5.2 considers strain hardening effect in the spheres under heavy loading for the deformable base boundary condition. And case 5.3 considers friction in the contact area for the rigid base boundary condition. The chapter has been divided into these three sections and initially the results for case 5.1 for predictions of contact force and area have been discussed in detail. Later sections of the chapter discuss the results for case (5.2) and (5.3).

Table 5.1: Table showing the boundary conditions used for the study

Case	Boundary condition	Strain Hardening	Friction
5.1	Deformable base & Rigid base case	NO	NO
5.2	Deformable base	YES	NO
5.3	Rigid base	NO	YES

5.1 Elastic perfectly plastic (No Strain hardening) results

The results of the described finite element model for the frictionless elastic-perfectly plastic behavior (shown in Fig. (5.1)) are now presented and also used to formulate closed-form models of heavily deformed spherical contact. Again, two cases based on the boundary conditions have been considered for different constraints at the base of the sphere namely,

- Deformable base
- Rigid base

The closed form models use the principle that during plastic deformation, volume is generally conserved (also used by Chang et. al. [5]) for formulation of equations for the deformed radius of the sphere. In the current study, finite element models to determine the effective instantaneous radius have been built for both the deformable and rigid base case at each penetration step. These effective instantaneous radius formulations can then be substituted for the value of R in the Jackson, Green and Marghitu model [22] in Eq. (13). This results in a closed form model providing more

accurate predictions of the contact pressure for the fully plastic contact. The current study also aims to extend the Jackson and Green model [4] to predict the contact radius and contact force for fully plastic contact.

In order to validate the simulation results with experimental data, a comparison with an existing experimental study of the same problem by Chaudri [2] was also performed. The results were plotted against this experimental data and a coefficient of correlation was calculated to show how well the current model predictions reflect on this data.

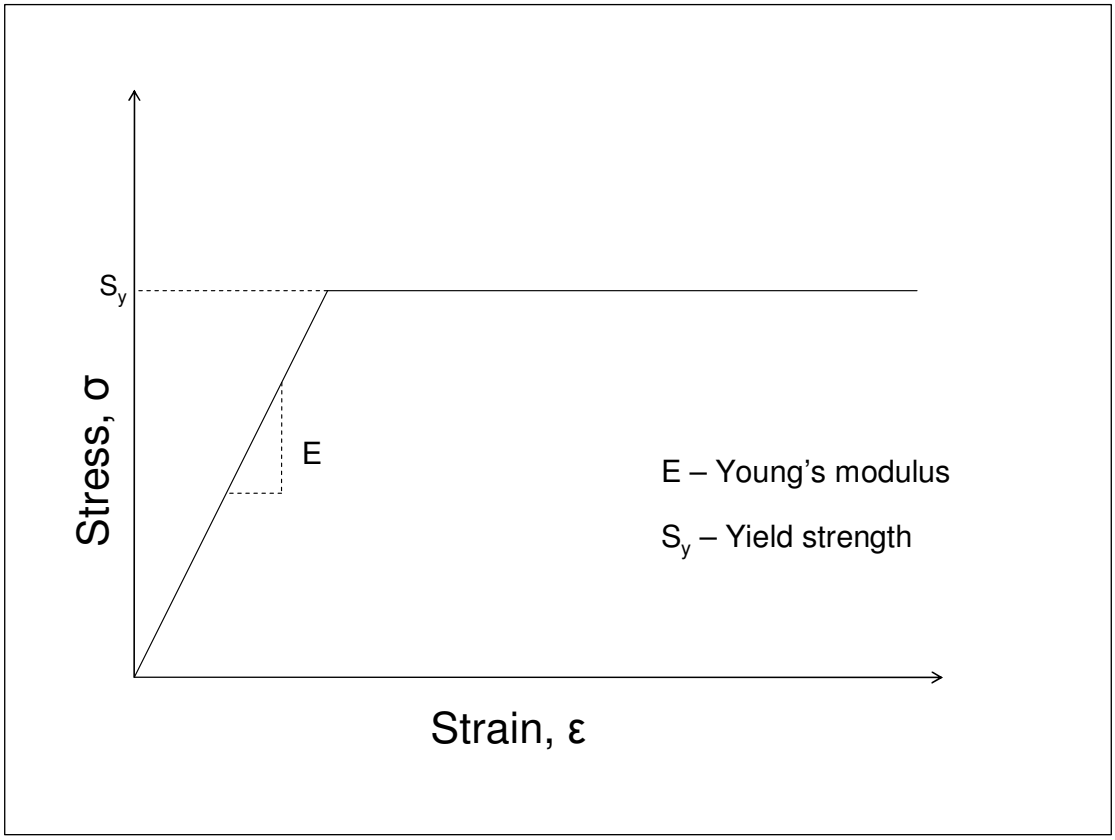

Figure 5.1: Stress strain curve for a material exhibiting elastic perfectly plastic behavior

5.1.a Theoretical calculation of the instantaneous radius

First, Case 1 (deformable base) for a hemisphere able to deform at the base in the radial direction is considered (Fig. 4.1a). This also corresponds to the case of a fully compressed 3-D sphere. When the sphere is flattening severely, the geometry shown in Fig. (4.1a) will be used. Assuming mostly plastic deformation occurs and that the volume is conserved, the initial volume and the deformed volume can be equated and solved to find the instantaneous radius of the sphere. It is also assumed that the spherical shape of the surfaces out of contact is always maintained even when the radius increases from an initial value of R to a deformed value of R_1, except that it will be truncated at the contact area. The deformed sphere can then be modeled to have the geometry of a hemisphere truncated by a flat surface. Therefore, the volume of the initial hemisphere before deformation is

$$V_1 = \frac{2\pi R^3}{3} \tag{18}$$

Likewise, the volume of a truncated hemisphere shape used to model the deformed sphere is

$$V_2 = \pi {R_1}^2 (R - \omega) - \frac{\pi}{3}(R - \omega)^3 \tag{19}$$

Using the volume conservation principle, setting V_1 equal to V_2 and solving for R_1 results in

$$R_1 = \sqrt{\frac{2R^3}{3(R-\omega)} + \frac{(R-\omega)^2}{3}} \tag{20}$$

Eq. (20) can be substituted into Eq. (13) for the radius, *R*. This will result in an improved prediction of the fully plastic contact pressure, as shown in Fig. (5.2). Using this modified radius in Eq. (13) results in a average difference between Eq. (13) and the FEM results of 4.78% with a maximum of 8.76%. Therefore the spherical contact equation provided by Jackson, Marghitu and Green [22] in Eq. (13) can be modified to consider deformation larger than *a/R* = 0.41 by substituting Eq. (20) into Eq. (13). It should be noted that the results for three different sets of material properties are shown. The three different material properties used in the analysis are *Sy/E* = 0.005, 0.0025, and 0.0001. This shows that the current non-dimensionalization scheme causes the results to collapse into one curve and the model works for several different materials. Eq. (20) predictions have been compared to the FEM results in Fig. (5.3). The average difference between the FEM and Eq. (20) predictions in about 1.1% for each material property and a maximum of 2.3%.

Figure (5.4) shows the pressure distribution across the contact area for increasing penetration. As can be seen in the figure, the contact pressure towards the end of the contact has a edge effect where the trend continuously seems to increase.

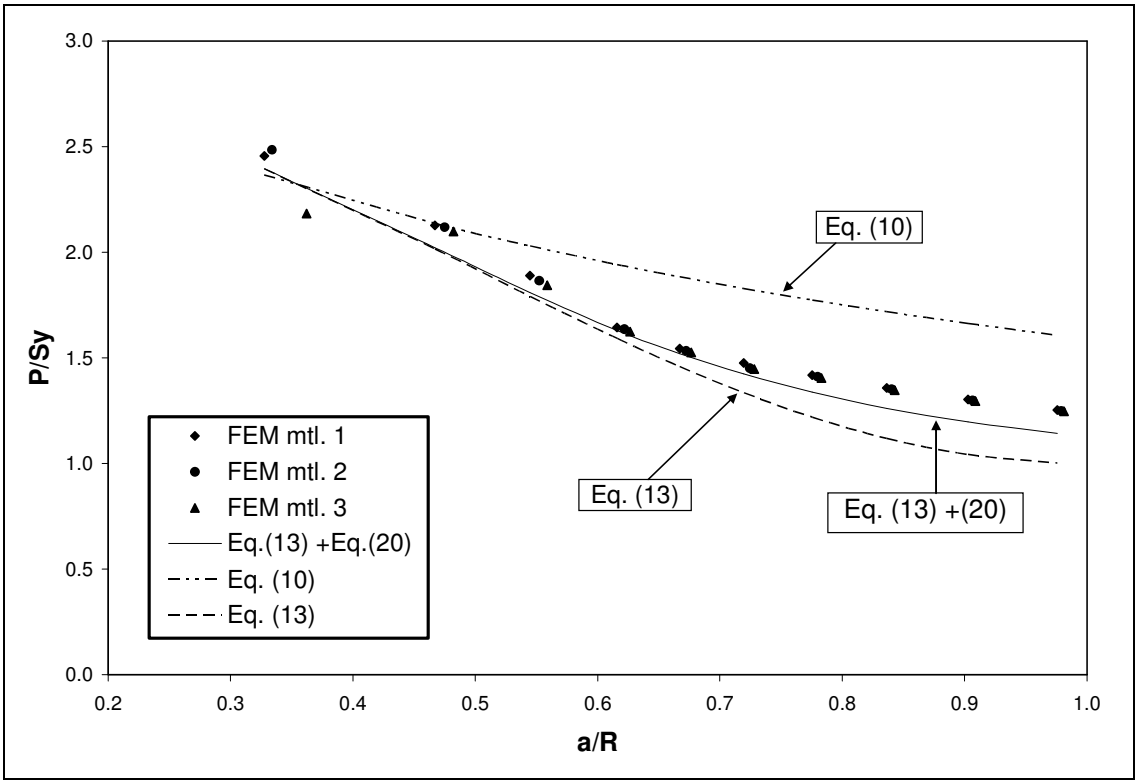

Figure 5.2: Comparison of predictions for case 1 (deformable base)

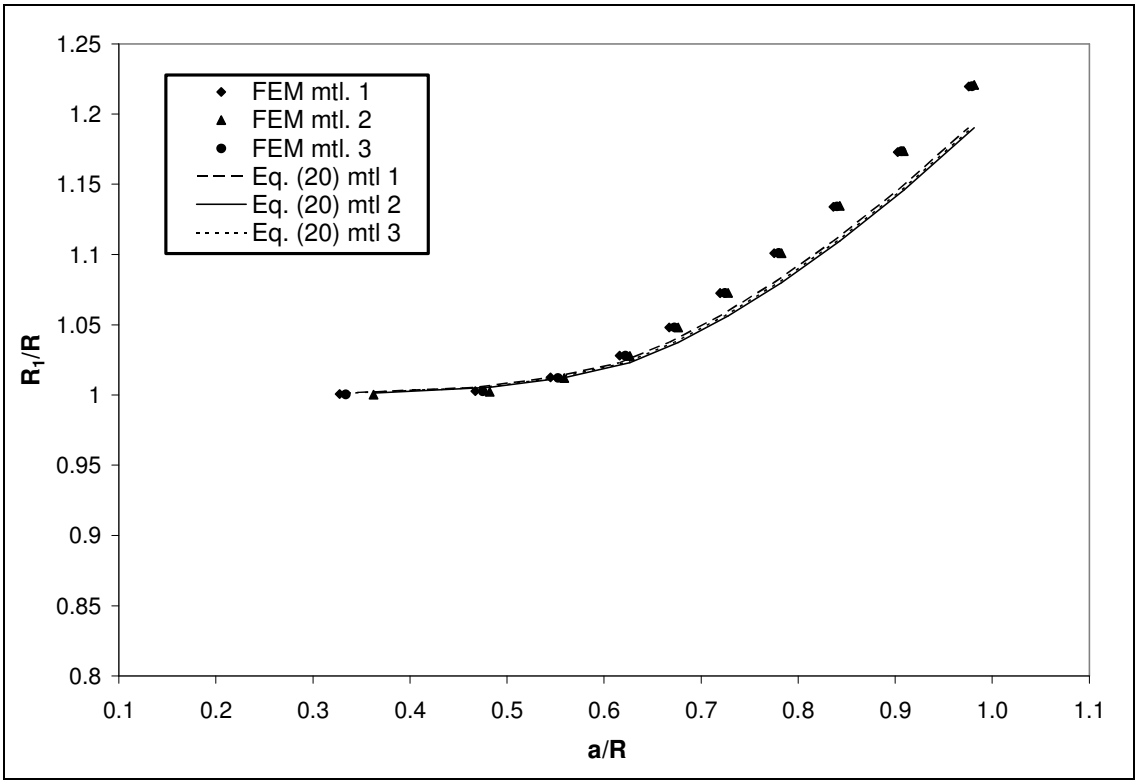

Figure 5.3: Comparison of FEM results with Eq. (20)

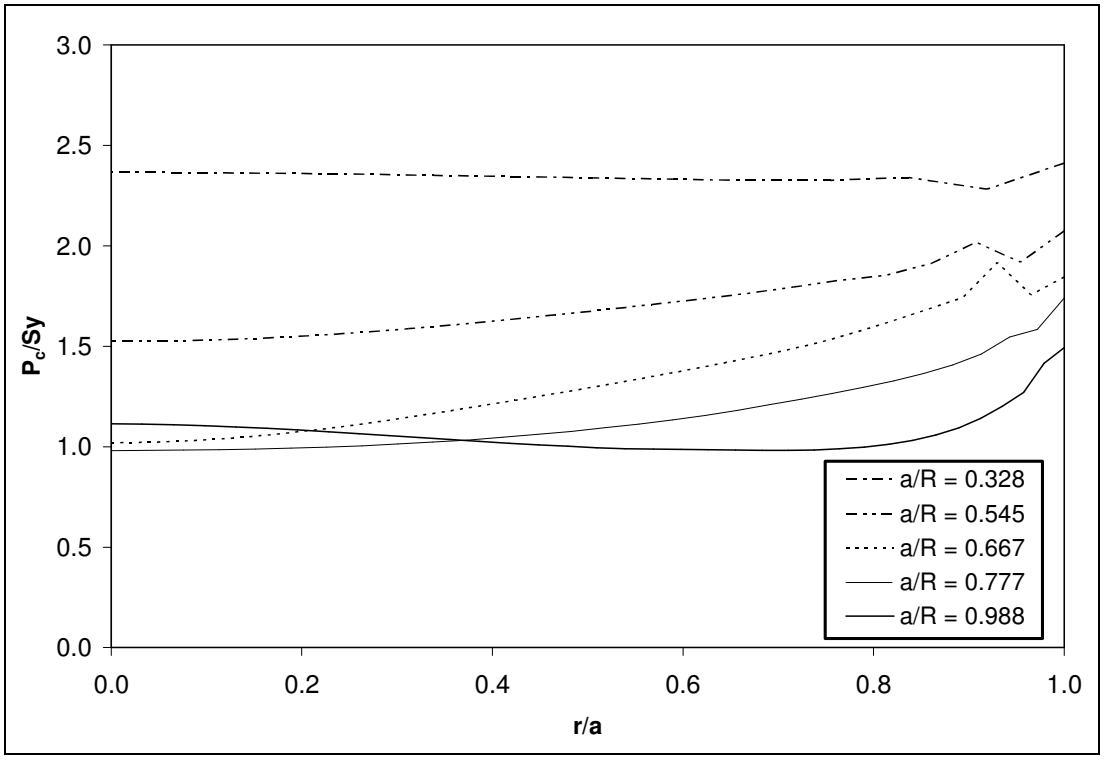

Figure 5.4: Pressure distribution across the contact area

For Case 2, the rigid base case, the current work borrows the barreling theory from S.Malayapam et al. [27] who give an equation describing the bulging of cylinders under compression. Figure (5.5) shows the geometric nomenclature of the barreling rigid base case. Note that it is assumed that even though the sphere deforms outward to bulge, the circular shape of the bulge is always maintained.

Just as with the deformable base case, the principle of volume conservation is applied and the volume of the sphere before deformation is set to the volume of the compressed hemisphere (modeled by the barreling shape shown in Fig. 5.5). This results in the following equation:

$$\frac{2}{3}\pi R^3 = \frac{\pi}{12}\left[2(2R_2)^2 + 4a^2\right](R-\omega) \tag{21}$$

Solving for the effective bulging radius, R_2,

$$R_2 = \sqrt{\left(\frac{R^3}{(R-\omega)} - \frac{a^2}{2}\right)} \tag{22}$$

For a better fit to the FEM data, Eq. (22) is modified with a constant δ so that

$$R_2 = \sqrt{\left(\frac{R^3}{\delta(R-\omega)} - \frac{a^2}{2}\right)} \tag{23}$$

Note that it is acceptable to include the constant δ because in actuality the case of a flattened sphere is not the same as a barreling cylinder in compression (although the final shape is similar). Unlike the case of cylinders, the vertical surfaces of the sphere have some curvature. The constant has a value very close to unity ($\delta = 0.76$), also showing that the overall inclusion of the constant only changes the quantitative predictions. The percentage error between the model (Eq. (13 and 23)) and the FEM results is an average of 2% and maximum of 4.6%. Fig. (5.6) shows the predictions of Eq. (13) using Eq. (23) in comparison to the unmodified Eq. (13) and Eq. (10). Clearly, Eq. (13) modified using Eq. (23) agrees better with the FEM results than Eq. (13) and Eq. (10). Fig. (5.7) shows the effectiveness of the constant by comparing Eq. (22) (without constant, δ) and Eq. (23) (with constant, δ) with the FEM results. The results are shown for three different sets of material properties (Sy/E = 0.005, 0.0025, and 0.0001). The deformed spherical geometry approaches the deformed cylindrical geometry as more and more deformation occurs and so the agreement between the theoretical volume conservation model Eq. (23) and FEM improves with more deformation.

Hence, the changing radius for the two cases of the sphere given by Eq. (20) and Eq. (23) have been used to modify Eq. (13) by substituting R_1 and R_2 in for R. It appears that this is the first time that these bulging and barreling effects have been observed and included in models of spherical contact. Fig. (5.8) shows the pressure distribution across the contact area during the rigid base case.

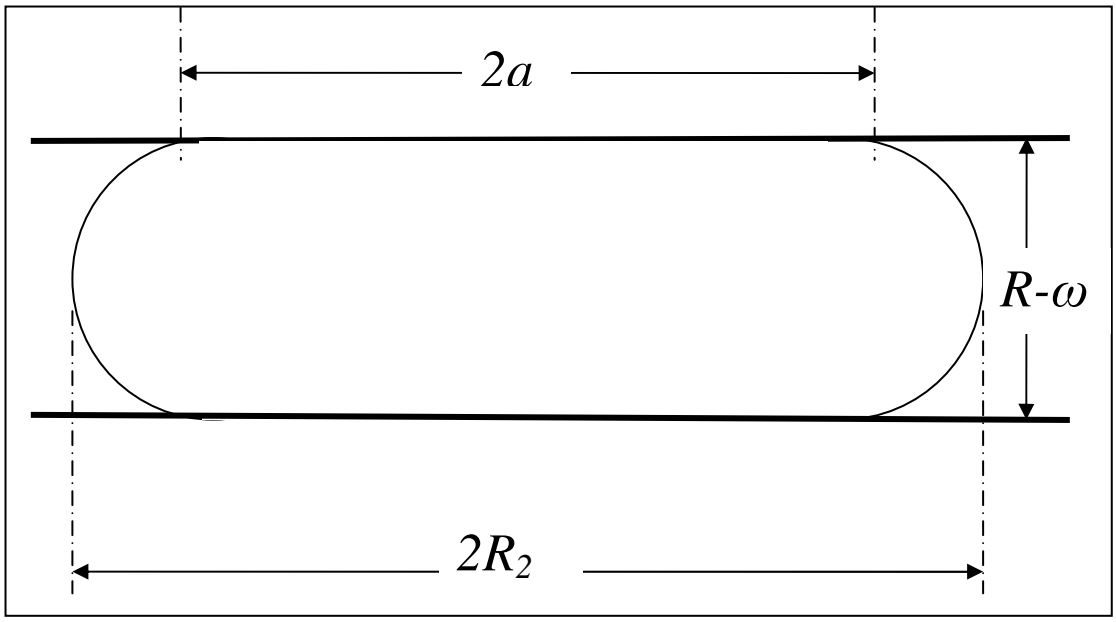

Figure 5.5: Nomenclature for the rigid base case

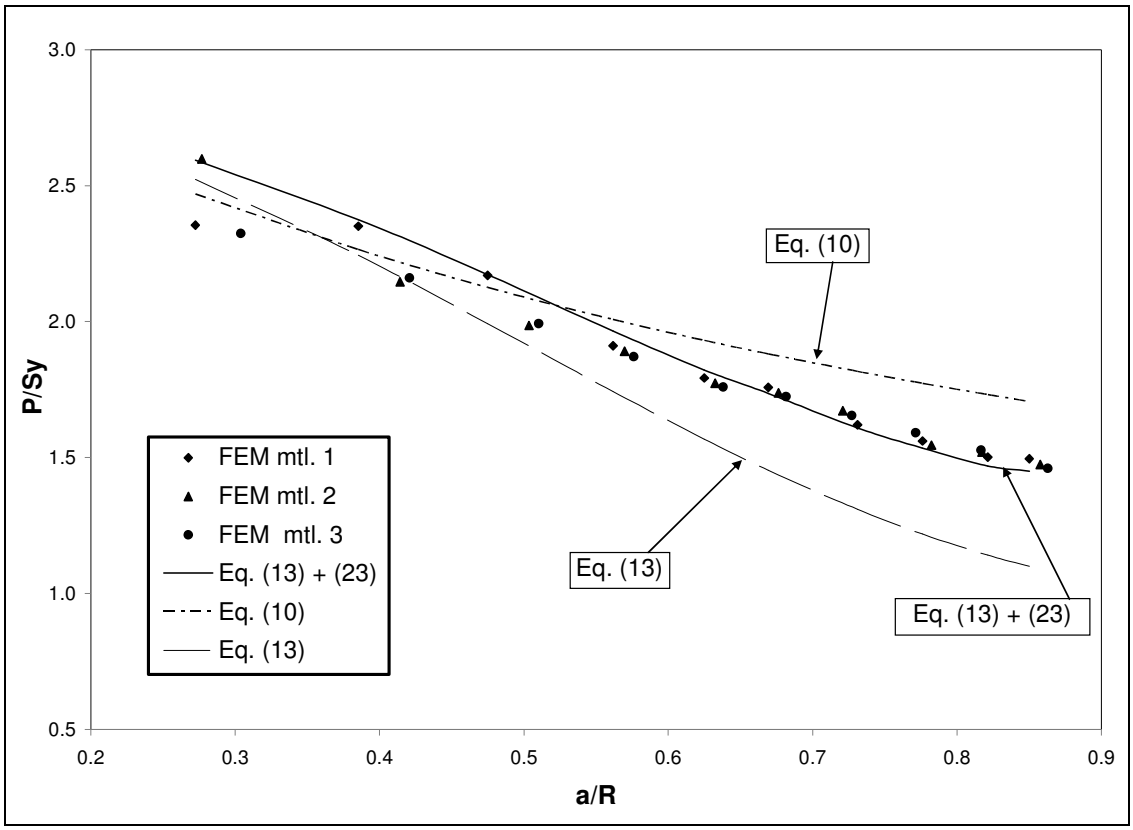

Figure 5.6: Comparison of predictions using barreling concept for case 2 (rigid base).

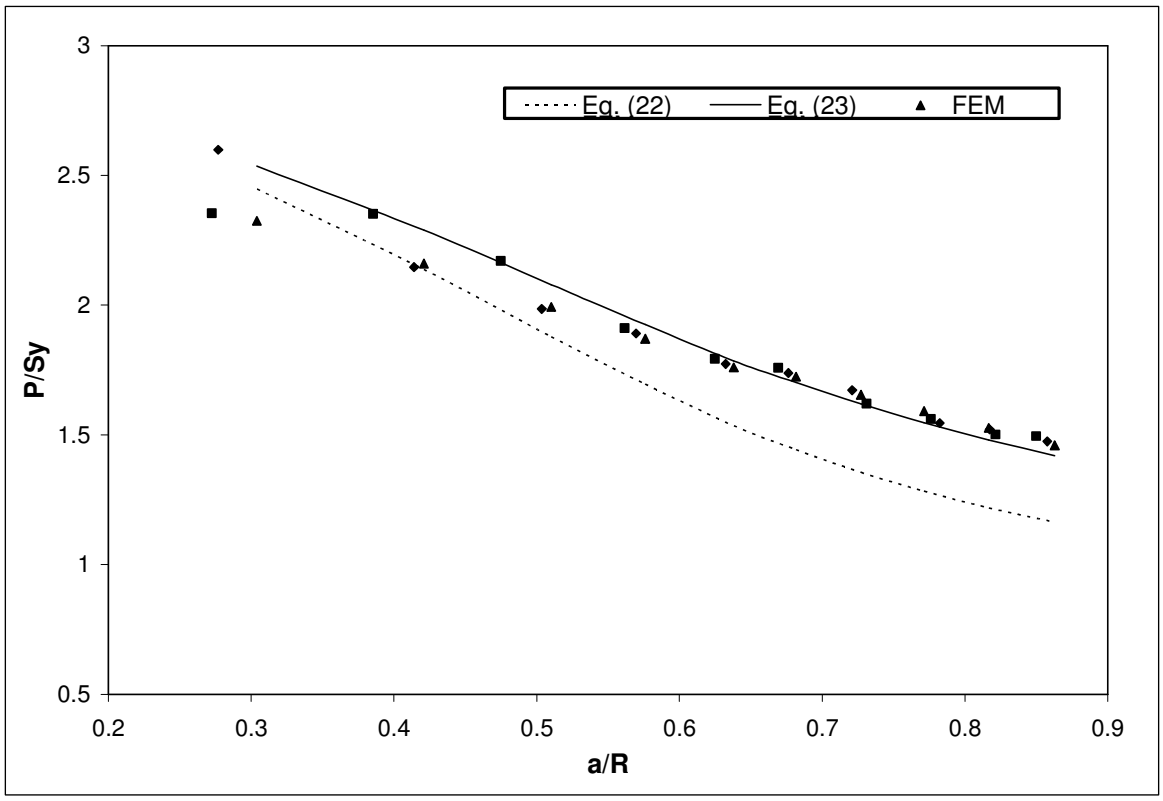

Figure 5.7: Effectiveness of δ (delta)

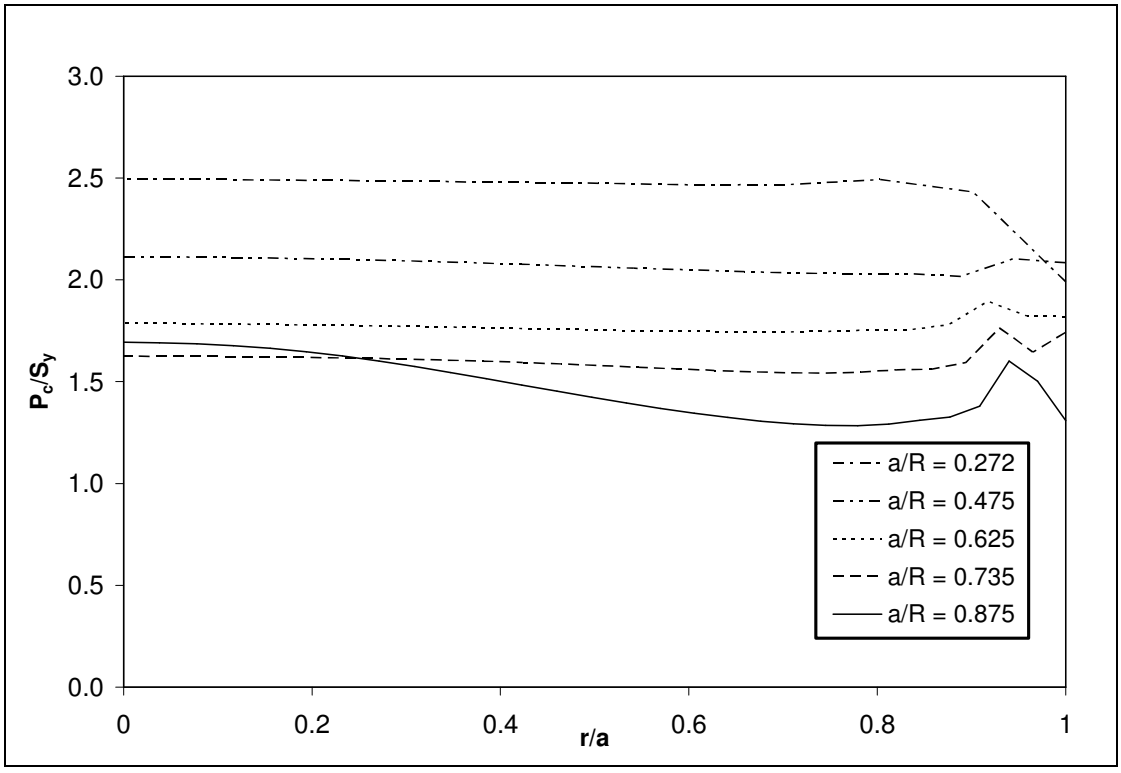

Figure 5.8: Pressure distribution across contact area

5.1.b Contact radius

Jackson and Green [4] gave Eq. (12) for the prediction of the contact radius during elasto plastic deformation. As mentioned previously these predictions are valid only until $a/R \leq 0.41$. The JG model did not consider the heavy loading of spherical surfaces. The current study aims to modify Eq. (12) and make it applicable not only to elasto-plastic but also to large fully plastic deformations where $a/R > 0.41$

Jackson and Green [3] provided the FEM data used to build the model in their work. Modifying Eq. (12) involves using both the JG data and the FEM results from current study. This is accomplished by fitting an equation to the FEM results of Jackson and Green [3] and the new FEM data acquired in this work that tracks surface deformation farther in the fully plastic regime. The equation provides a relationship between the contact radius and penetration. For the deformable base case, the resulting fit equations differ from all the FEM results by an average of 5% and are given as,

$$\left(\frac{a}{R}\right)_{new} = \left(\frac{a}{R}\right)_{JG} + A_1\left(\frac{\omega}{\omega_c}\right)^2 - A_2\left(\frac{\omega}{\omega_c}\right) \tag{24}$$

where $\left(\frac{a}{R}\right)_{JG}$ is given by Eq. (5) and

$$A_1 = 0.0826 \cdot \left(\frac{S_y}{E}\right)^{3.148} \quad ; \quad A_2 = 0.3805 \cdot \left(\frac{S_y}{E}\right)^{1.545}$$

The normalized contact radius (*a/R*) predicted by Eq. (24) is compared Jackson and Green [4] and FEM results in Fig (5.9) and (5.10). The results have been divided into 2 figures for small and large deformations. Small deformations are defined till *a/R =0.41* and large deformations extend till *a/R=1*. Note that the material properties of both sets viz. JG model and current study, of data are slightly different (see Table 5.2).

Table 5.2: Material properties used in (a) Jackson and Green [3] and (b) the current FEM analysis.

Material	Yield strength, (S_y) GPa	Equivalent modulus of elasticity (E') Gpa
1a	0.9115	228.2
1b	1	228.2
2a	0.5608	228.2
2b	0.5	228.2
3a	0.21	228.2
3b	0.2	228.2

Mayuram and Megalingam [23] also built a elasto plastic spherical contact model, essentially studying the same problem. They provide a set of equations to predict the contact area and contact force during elastic, elasto-plastic and fully plastic deformations. These equations are valid till $\omega/\omega_c = \infty$ and are given previously in this work. In order to compare the contact area given by the MM model, the equations for contact area are converted to give contact radius by substituting critical area equation as shown here for one of the penetration ranges defined by Eq. (14) resulting in,

$$\frac{a}{R} = \sqrt{\frac{A_c}{\pi R^2}} \tag{25}$$

As shown in Figs. (5.9) and (5.10), the JG model (Eq. 12) and MM model (Eq. 25) model compare well for very small values of *a/R* but as the contact radius increases, the predictions progressively depart from the FEM results.

It appears that Eq. (25) is limited to smaller deformations (see Fig 5.9) and as the deformations get larger, the model does not seem to agree with the FEM results (see Fig.5.10). The current study (Eq. 24) does not compare as well as the JG model Eq. (12) to the FEM data at lower interferences (see Fig. (5.9), but for large interferences Eq. (24) compares much better with the current FEM results. The percentage difference between the current and JG model for small interferences is a maximum of 5.18% and a minimum of 1%. The trend seems to be the same for all the three material properties used for the study.

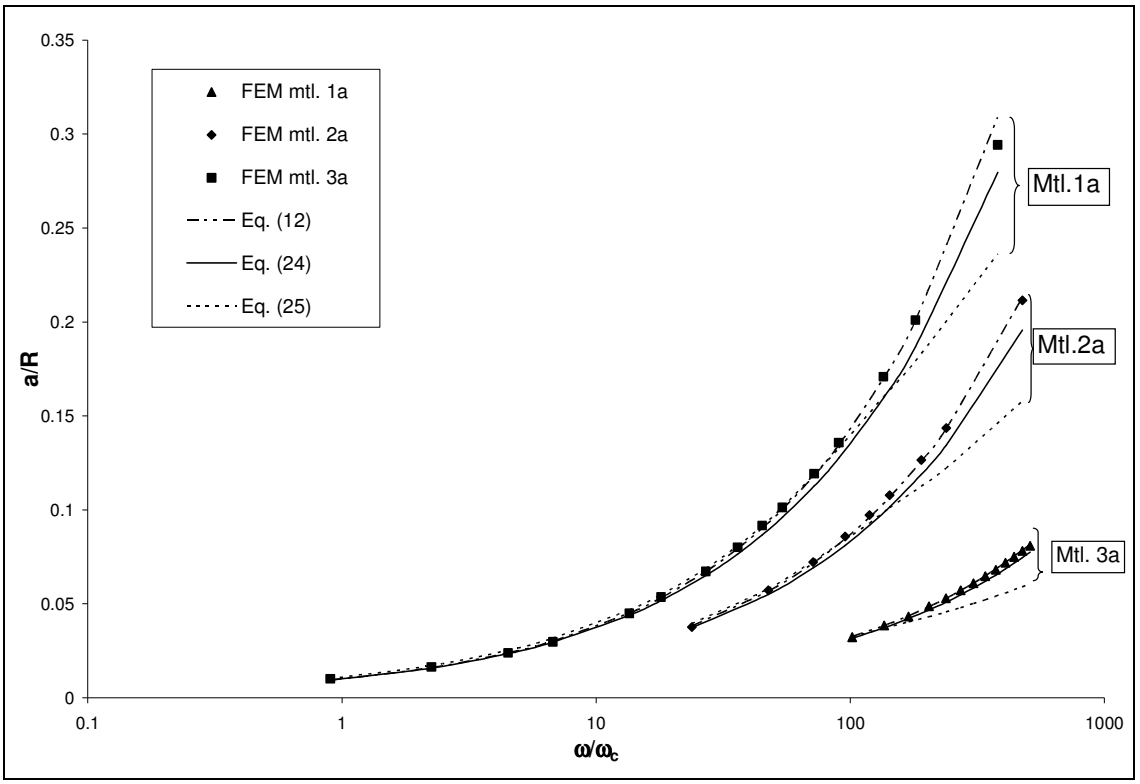

Figure 5.9: Comparison of predictions of Eq. (12), (24) and (25) with FEM results for the deformable base case for small values of penetration.

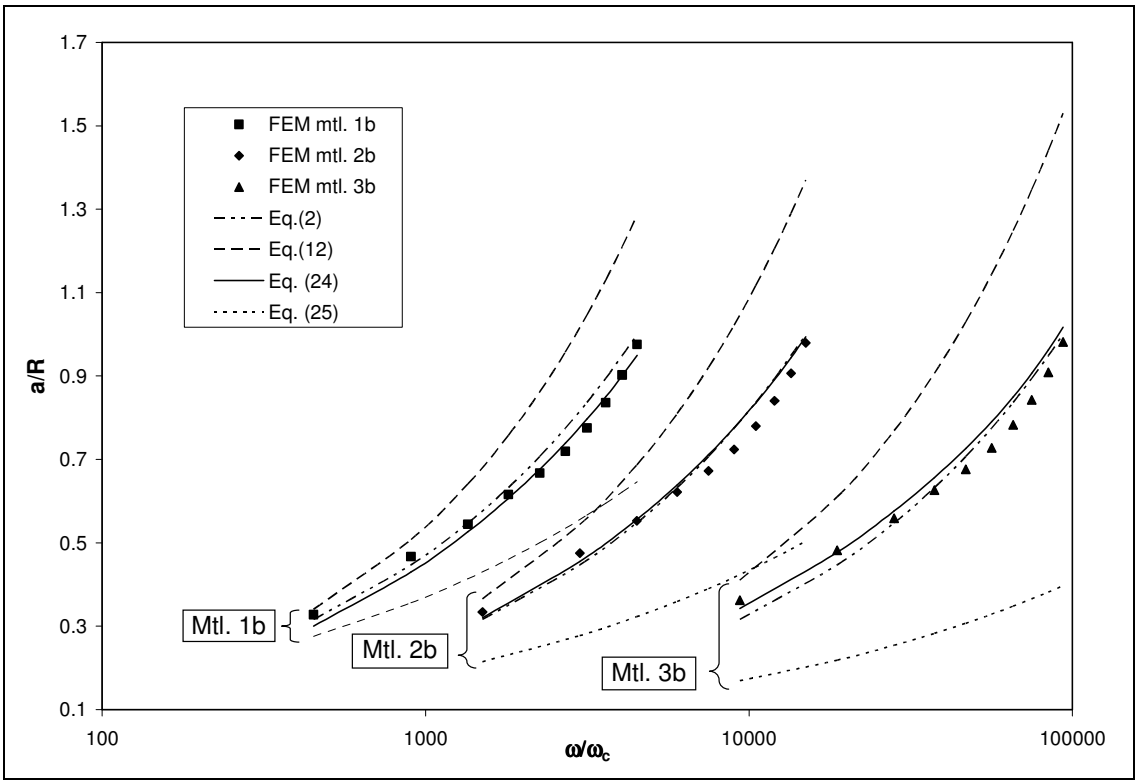

Figure 5.10: Comparison of predictions of Eq. (12), (24) and (25) with FEM results for the deformable base case for large values of penetration.

For the rigid base case (case 2), equations describing the ratio between the contact radius and spherical radius are also fit to the FEM data of Jackson and Green [3] and the current work using the same form given in Eq. (24). The resulting fit equations for the rigid base case differ from the FEM data by an average of 2.5% and are given as

$$\left(\frac{a}{R}\right)_{new} = \left(\frac{a}{R}\right)_{JG} - A_3\left(\frac{\omega}{\omega_c}\right)^2 - A_4\left(\frac{\omega}{\omega_c}\right) \tag{26}$$

where,

$$A_3 = 158393\left(\frac{S_y}{E}\right)^{5.605} \quad ; \quad A_4 = 0.0034\left(\frac{S_y}{E}\right)^{0.8939}$$

Figs. (5.11) and (5.12) show the predictions of the current model for the rigid base case (Eq. 26) compared with the FEM, JG and MM models. Again, for clarity the results are presented for two different penetration levels in Figs. 5.11 (for small interferences) and Fig. 5.12 (for large interferences). The results show trends similar to the deformable base case, that, for small deformations, the Jackson and Green [4] model (Eq. (12)) compares the best with the FEM results. This is expected since the JG model is meant for only elasto plastic deformations. But the most interesting observation is that the model almost replicates the FEM data for small deformations. The MM model [24] results deviate significantly from the FEM at fairly small values of interference. From Fig. (5.12), it is very evident that the current model (Eq. 26) predictions are the most accurate when compared to the FEM results when large deformations occur.

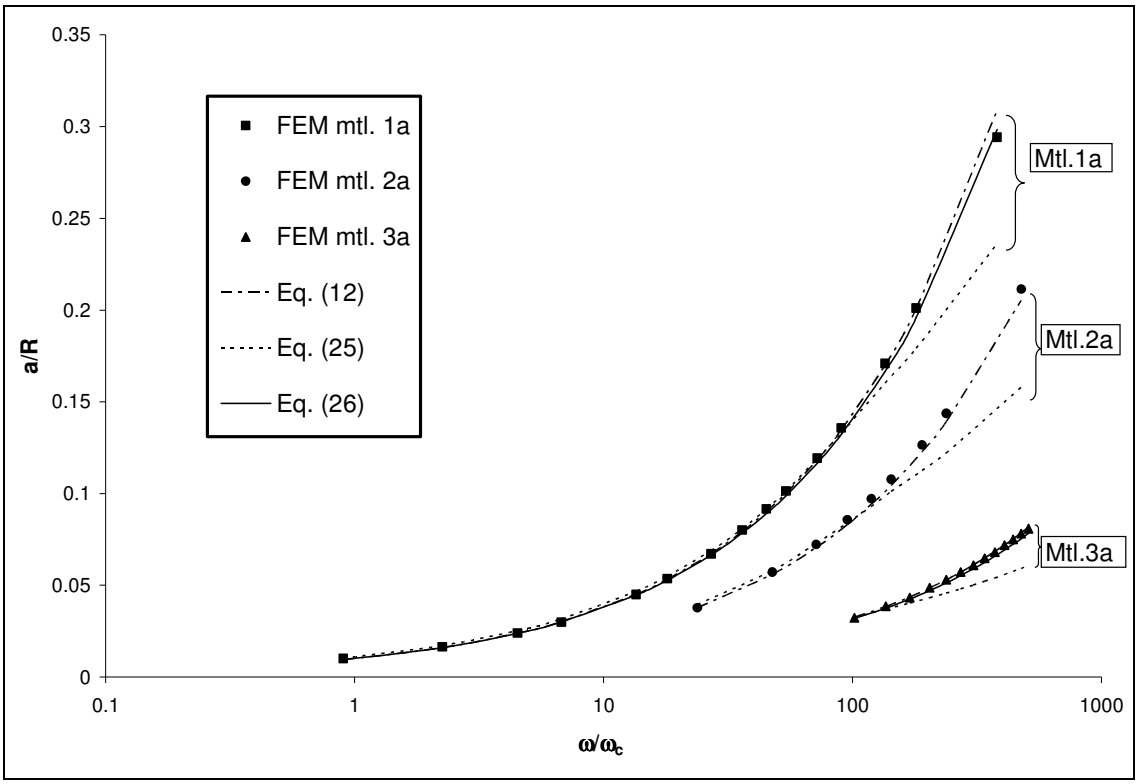

Figure 5.11: Comparison of predictions of Eq. (12), (25) and (26) with FEM results for the rigid base case for small values of penetration.

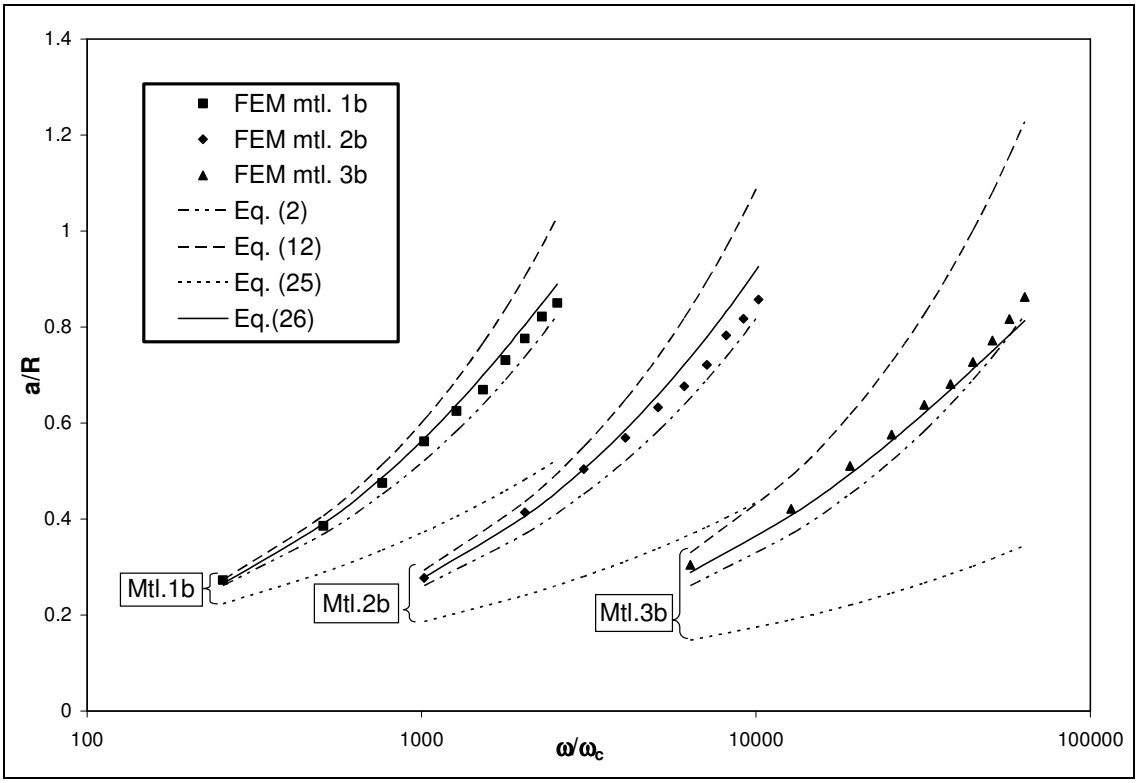

Figure 5.12: Comparison of predictions of Eq. (12), (25) and (26) with FEM results for the rigid base case for large values of penetration.

5.1.c Contact force

Jackson and Green [3] provide an equation for the contact force during elasto plastic deformations of a sphere valid up to *a/R*=0.41 (see Eq. (11)). The current work aims to provide an extended model that is capable of producing accurate predictions of the contact force by modifying Eq. (11) and extending it into the fully plastic deformation range. As deformations get larger, the first term in Eq. (11) approaches zero and the second term involving the contact pressure becomes dominant in predicting the contact force. The current study proposes that the contact pressure should be multiplied by the contact area for accurate predictions of the contact force, resulting in the following modified equation:

$$\frac{F}{F_c} = \left[\exp\left(-\frac{1}{4}\left(\frac{\omega}{\omega_c} \right)^{\frac{5}{12}} \right) \right] \left(\frac{\omega}{\omega_c} \right)^{\frac{3}{2}} + \frac{P}{F_c} \pi R^2 \left(\frac{a}{R} \right)^2_{new} \left[1 - \exp\left(-\frac{1}{25}\left(\frac{\omega}{\omega_c} \right)^{\frac{5}{9}} \right) \right] \qquad (27)$$

Eq. (11) does not contain a term which can address the increasing contact area during plastic deformations. Also, the value of *P* in Eq. (11) is calculated using Eq. (10) which has already been proven to give inaccurate predictions for fully plastic contact pressure with large deformations.

The new equation proposed in Eq. (27) uses the new contact area calculated from Eq. (24) and (26) .The contact pressure *P*, is calculated by modifying Eq. (13) for contact pressure predictions.

First the predictions of Eq. (27) for case 1 (the deformable base) have been shown in Figs. (5.13) and Fig. (5.14). Fig. (5.13) shows the comparison in the range of the FEM data provided by Jackson and Green (small deformations up to $a/R = 0.41$) and Fig. (5.14) shows the comparison in the range of the new FEM data (large deformations up to $a/R = 1$) from the current work. Comparisons of the current model with FEM results in Figs (5.13) and (5.14) reveal that the current model for contact force compares very well for both small and large interferences. For small interferences the current model predictions and Eq. (11) are almost indiscernible and so the predictions of Eq. (11) are not shown. As the deformations get larger, as shown in Fig. (5.14), the differences between the FEM results, the current model, Eq. (11), and Eq. (15) become very profound. In fact, the differences between the FEM results, the current model and the MM model (Eq. (15)) appears to sometimes be several orders of magnitude. Overall the current model performs well and better than the other models at predicting the contact force over the considered range of interferences. It is also interesting to note that the new equations capture some interesting trends in the force-interference curves shown in Fig. 5.14 for the rigid base case. There is a slight‘s’ shape to the FEM results that the new model equations also successfully capture.

* *The current model is a combination of Equations depending upon the case considered.*

For the Deformable base case, the current model is a combination of Eq. (13), (24) and (27). And for the rigid base case it is a combination of Eq. (13), (26) and (27).

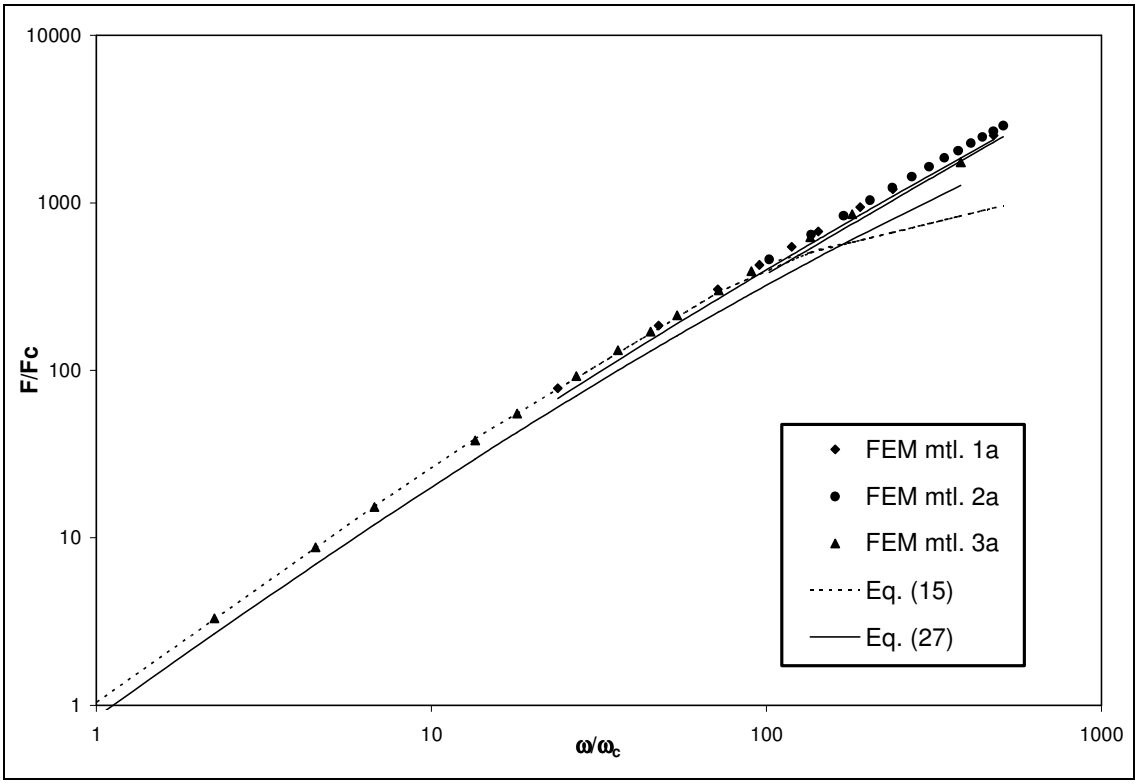

Figure 5.13: Comparison of predictions of contact force according to Eq. (15) and (27) with FEM results for the deformable base case with small loads

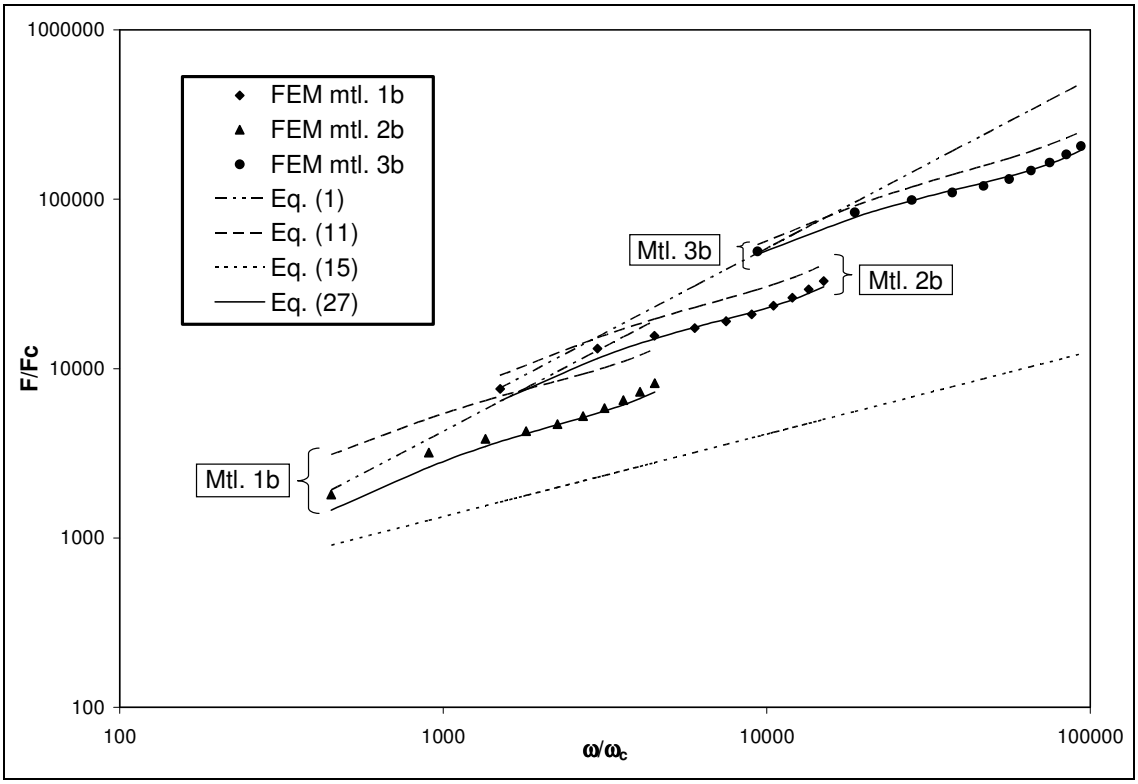

Figure 5.14: Comparison of predictions of contact force according to Eq. (11), (15) and (27) with FEM results for the deformable base case with heavy loads

Next, the current model of contact force for the rigid base case using Eqns. (13, 26 and 27) is compared to the FEM data and the previous models given by JG (Eq. (11)) and MM (Eq. (15)) as shown in Figs. (5.15) and (5.16). It is expected that the JG model (Eq. (11)) works better for the rigid base because they have studied asperity contact which is similar to the rigid base case. As seen from the comparison with the FEM results in Fig. (5.15) and (5.16), this is especially true when deformations get larger (*a/R* approaches 1). The observed trends for deformable and rigid base case in figs. (5.15) and (5.16) are significantly different.

The plots also show that the model by Megalingam and Mayuram [23] (Eq. (15)), significantly underpredicts the FEM results for large deformations. As expected, the new equations based on barreling and volume conservation agree well with the FEM results.

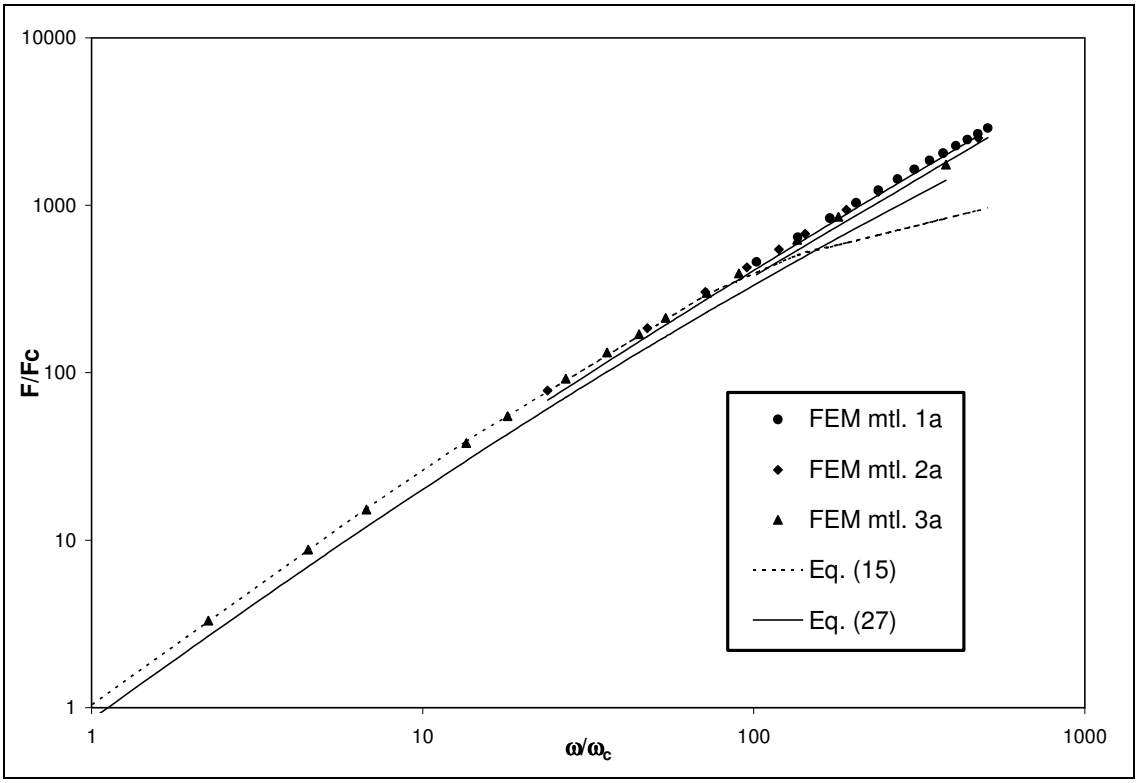

Figure 5.15: Comparison of predictions of contact force according to Eq. (15) and (27) with FEM results for the rigid base case with small loads

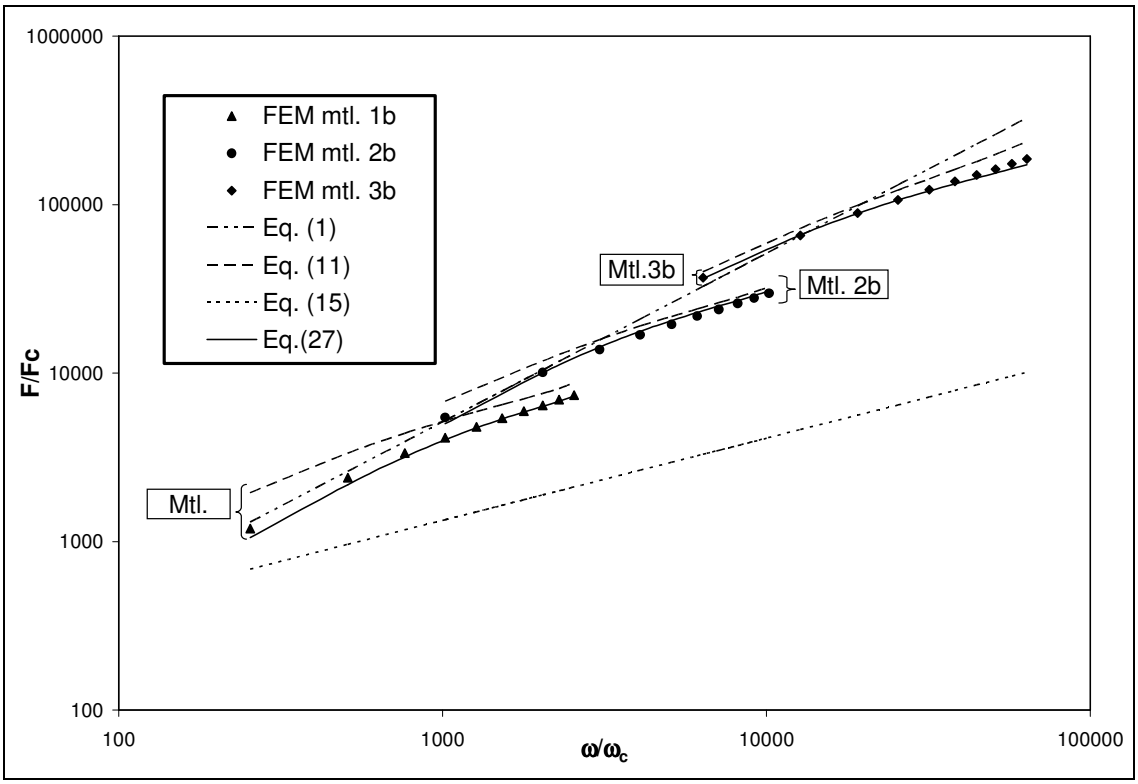

Figure 5.16: Comparison of predictions of contact force according to Eq. (11), (15) and (27) with FEM results for the rigid base case with large loads

5.1.d Comparisons with Existing Experimental Measurements

In order to validate the current model predictions for contact pressure and contact radius, the results were compared with experimental data measured by Chaudhri et al. [2]. They reported experimental results for the compression of metal spheres of different material properties (phosphor bronze, aluminum and brass) between two smooth parallel platens. The deforming geometry of the spheres in this experiment can be correlated to the deformable base case (case 1) in the current work.. The spheres used in the experiment were brass, aluminum and phosphor bronze all with diameters of 3.175mm. The current work compares the new model results with the results for the brass and phosphor bronze spheres given by Chaudhri [2] since the resulting *a/R* ratios for these tests are in the range of the current study compared to aluminum. The phosphor bronze spheres were work hardened in an attempt to cause there behavior to be like an elastic-perfectly plastic material when compressed under heavy loads. This was done to allow for comparison with existing models which mostly assume the material to behave elastic-perfectly plastically. The current model has also been modeled intially as elastic-perfectly plastic in the FEM simulations.

Measurements of Vickers hardness were provided by [2] before and after compression. A Leitz microhardness testing machine with an accuracy of ± 4% and a load of 50 gms-force (0.49 N) was used. This information has not been mentioned in their work, but a thorough literature survey of the equipment used in the experiments was done to find the accuracy of the results.

According to the hardness measurements following data has been given by Chaudhri [2].

Table 5.3: Material properties and Microhardness measurements as given by Chaudhri et al. [2].

Material	**Poisson's Ratio, υ**	**Elastic modulus, E (GPa)**	**Hardness (GPa)**	
			Before compression	After compression
Phosphor bronze	0.35	115	2.72 ± 0.06	2.68 ± 0.06
Brass	0.37	120	1.8 ± 0.08	2.22 ± 0.08

Using these values of hardness and standard values of elastic modulus for brass and phosphor bronze, a comparison is made between the predictions of the current model for the deformable base case and the experimental results [2]. In dimensional form the current model for the deformable base case is given as,

$$P = \left(2.84 - 0.92\left[1 - \cos\left(\pi \left(\frac{a}{R} \right)_{new} \frac{R}{R_1} \right) \right] \right) S_y \tag{28}$$

where, R_1 is calculated using Eq. (10), $(a/R)_{new}$ is calculated from Eq. (24), and R is the original radius of the sphere.

The value of the yield strength is not explicitly provided by Chaudhri et al. [2]. Instead it has to be calculated using the Vicker's hardness measurements given in table 5.3. Vicker's hardness measurements conducted by [17], [31] and [33] revealed that the value of the constant c, is between 2.8 to 3.3. These results have been found for frictionless compression experiments (similar to the current study). The current work

finds a value which H/Sy = 3.15 provides a trend closest to the experimental results given by Chaudhri [2] for phosphor bronze and brass. The results have been presented in Figs. (5.17) and (5.18). The data compares the predictions of the current model for three different values of the constant ,*c* (2.8, 3.15 and 3.3).

The experimental data given by Chaudhri et al. [2] was extracted using DataThief©. The predictions of the current model (Eq. 28) are compared with this extracted data and are shown in Figs. (5.17) and (5.18). The trends of the experiments and model are qualitatively and quantitatively very similar. The average error between the model and the measurements is about 9% for the brass results and 7% for the phosphor bronze. Considering that in reality there is some hardening and friction occurring in the tests that is not considered by the model, this shows surprisingly good agreement between them.

The R-squared value to determine the co-efficient of correlation between the experimental data and the current model has also been calculated. For the case where *c* is 3.15, the R-squared value for the correlation was found to be 0.9851 and 0.9707 for phosphor bronze and brass respectively. The R-squared value shows how closely the trends of the results being compared are related to each other. The maximum R-squared value is unity. As mentioned previously, the phosphor bronze spheres were work hardened to achieve newly elastic perfectly plastic behavior. For Phosphor bronze, the percentage error between the experimental the current model is observed to be lower and the R-squared number is higher compared to brass. This is because the current model is simulated as elastic perfectly plastic sphere and phosphor bronze shows a behavior closest to this (see table. 5.3).

This suggests that the new model presented in the work can be used effectively to predict the behavior of heavily deformed spheres, especially when a material has little strain hardening. Strain hardening and friction which add complexity to the problem have not been considered in this section but has been discussed later. The study by Chaudhri [2] also mentions the possibility of a barreling mechanism for predicting the deforming geometry of spheres during compression. The current study has studied this possibility in detail and confirms these possibilities in the previous sections.

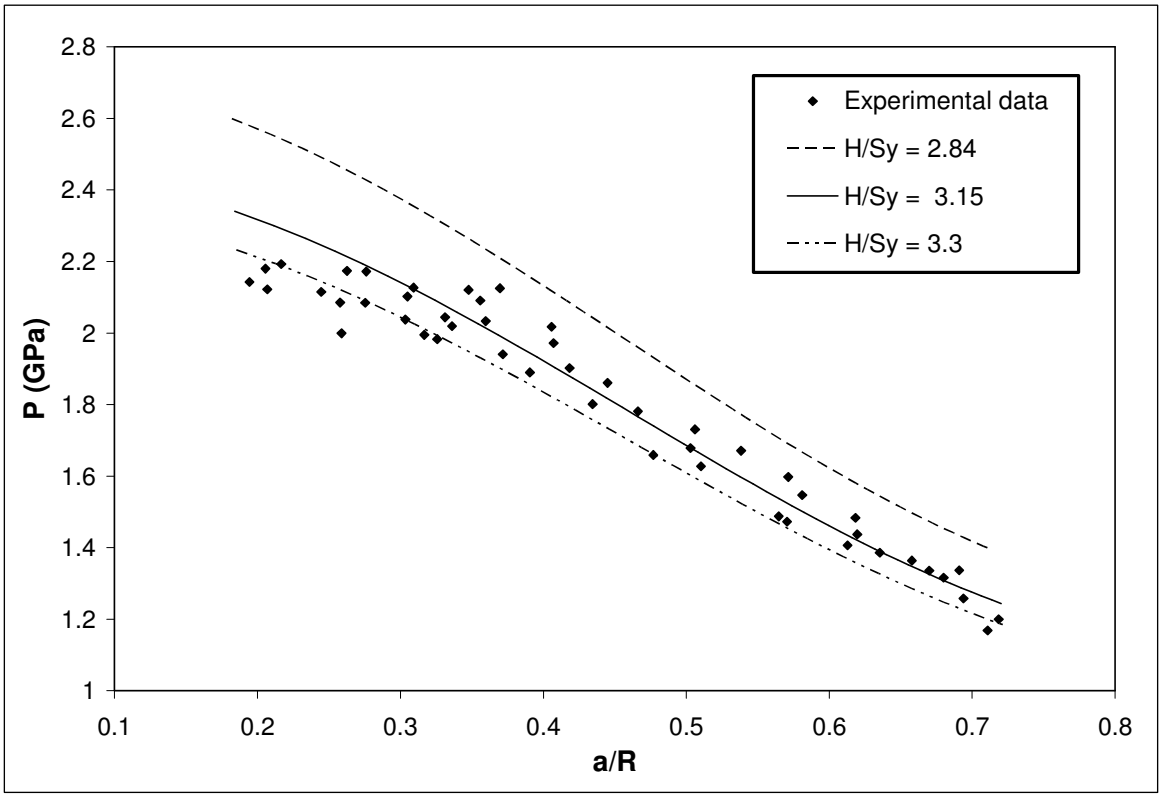

Figure 5.17: Comparison of experimental and simulation based model for phosphor bronze material

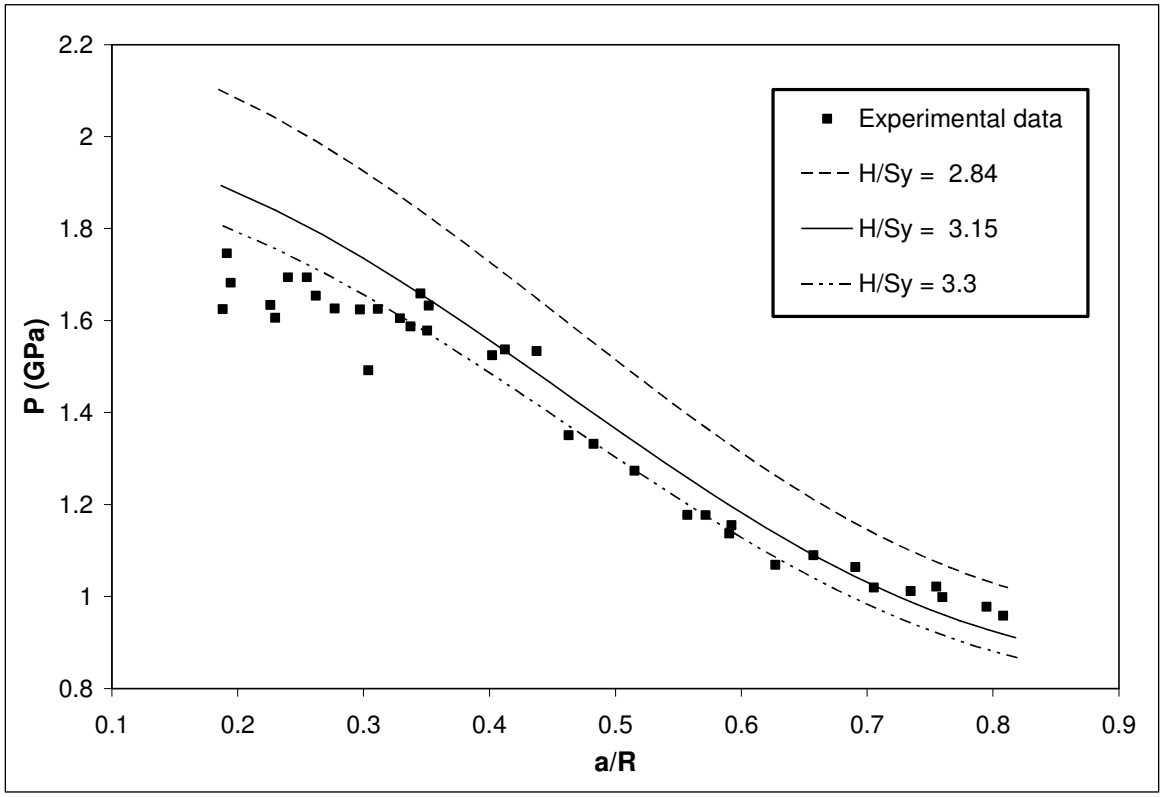

Figure 5.18: Comparison of experimental and simulation based model for brass material

5.2 Effects of strain hardening

Strain hardening also known as work hardening occurs when metals undergo plastic deformation. The material essentially gains resistance to permanent deformations. This happens because the material gets saturated with dislocations which prevent formation of any more dislocations. The current study has to this point not considered strain hardening in the sphere under compression. However in reality there will be some strain hardening in almost all metallic materials.

Therefore an attempt was made to model the sphere under compression while including strain hardening effects. The current work compares its simulation results with the maps of microhardness distribution provided by Noyan [1] at various levels of penetration and draws some interesting observations and conclusions. Noyan [1] conducted experiments by compressing spheres and measuring the hardness across the sphere and mapped these microhardness values throughout the depth of the sphere for 4%, 11%, 20% and 58% compressive macroscopic strain. Compressive strains are the difference between the initial (undeformed) and final compressed height of the sphere. The sphere is divided into zones depending on the hardness measured. This gives an exact idea of the birth and progression of stress distribution in the sphere. He also concluded that the area of contact and the area at the centre of the sphere are independent of material if sphere and the size.

In the finite element analysis, strain hardening is introduced into the spheres by varying the tangent modulus of the material. The current work considers tangent modulus of 1%, 2% and 4% hardening of the material. Discussions with other scholars in this field

who have conducted experiments to study strain hardening revealed that hardening reaches values upto 4% during compression tests. The compressive strain considered by Noyan [1] reach a maximum value of 58%. The current study considers compressive strains upto 50%. Hence, the Von Mises stress distribution for the various levels of strain hardening in the current study can be compared with almost all of the microhardness plots given by Noyan [1]. The FEM predictions of contact pressure at 0%, 1%, 2% and 4% tangent moduli strain hardening are given in Fig. (5.19).

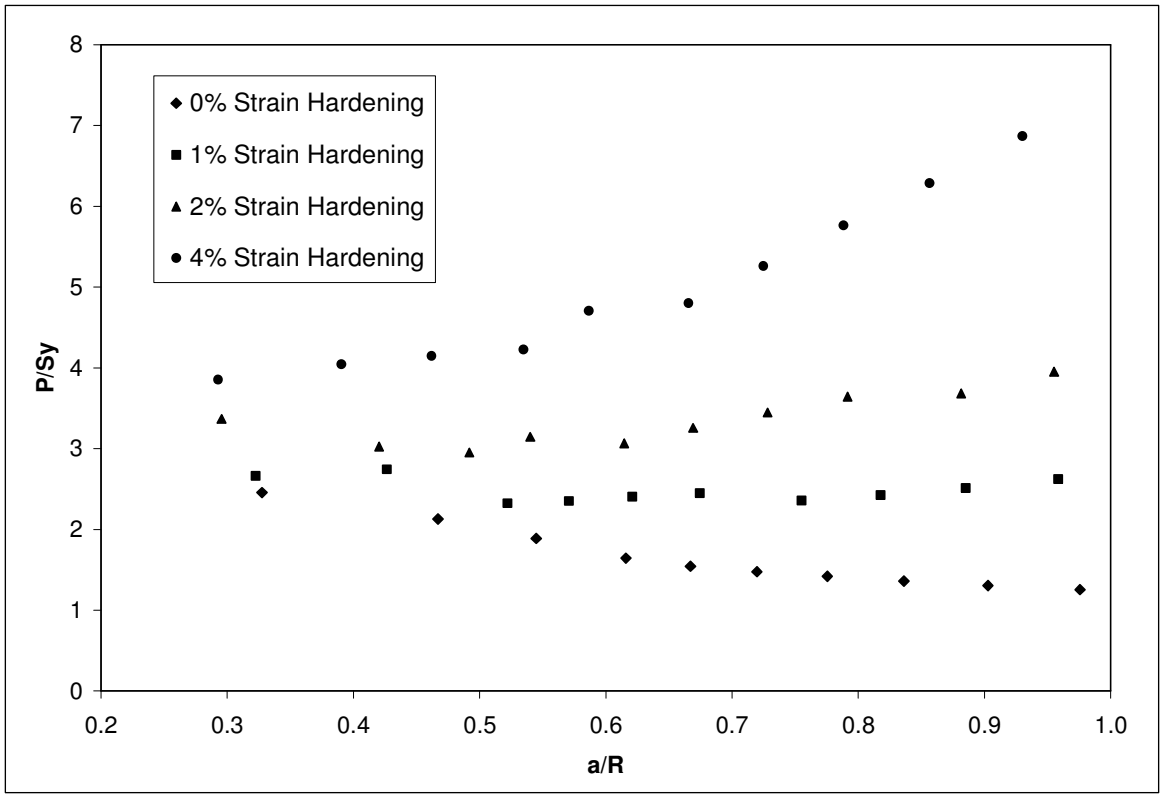

Figure 5.19: Variation of contact pressure with increasing contact radius

The inclusion of hardening appears to neglect the geometric effects on hardness during spherical flattening (see [7],[2]). Essentially, hardening counteracts the trend of Eq. (13) causing the H/S_y to increase instead of decreasing as a/R increases. This may be why this phenomenon had not been experimentally recognized until Chaudhri et al. [2].

In order to study the mapping of the stress distribution inside the sphere, the Von Mises stress distribution at each load step is mapped and shown in Figs. (5.20) and (5.21) and (5.22). The figures show Von Mises stresses for one material with three different levels of strain hardening (4%, 2% and 0%). The trends suggest that the maximum Von Mises stress zone for 4% and 2% strain hardening cases in Figs. (5.20) and (5.21) migrates from just below the contact surface to the center of the sphere. These results have been compared with the experimental work presented by Noyan [1]. The comparisons reveal similar trends in both the studies. The zone indicating maximum Von Mises stress levels represented by the red zone in Figs. (5.20) and (5.21) can be compared to the 'C' zone in the experimental work by Noyan [1]. In this experimental work by Noyan [1], the sphere is divide into zones based on microhardness measurements and 'C' zone is the hardest zone. As the compressive strain increases the 'C' zone increases in size and migrates to the center of the sphere similar to the current observations in Figs. (5.20) and (5.21).

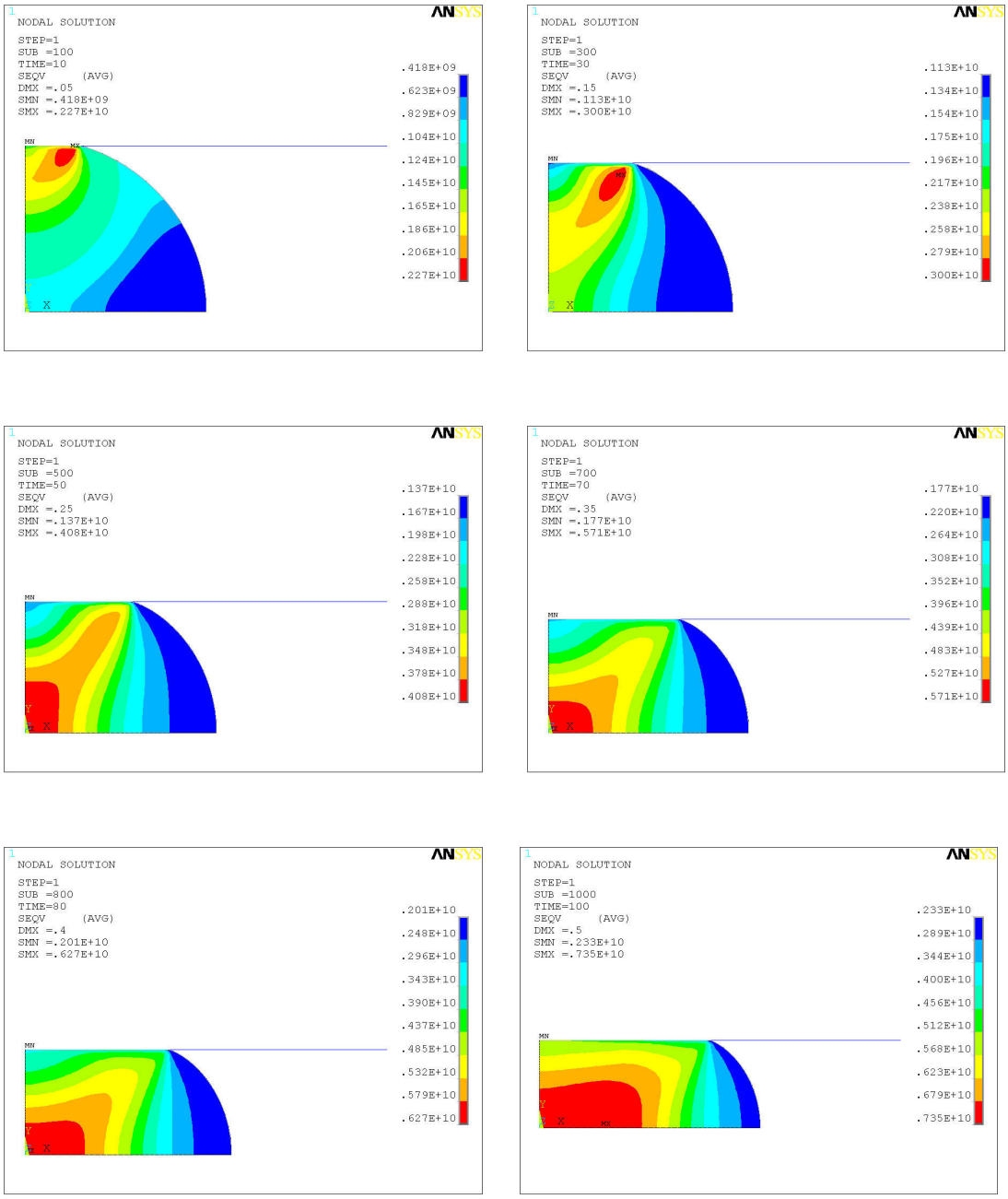

Figure. 5.20: Von Mises stress distribution for 4% strain hardening in the sphere.

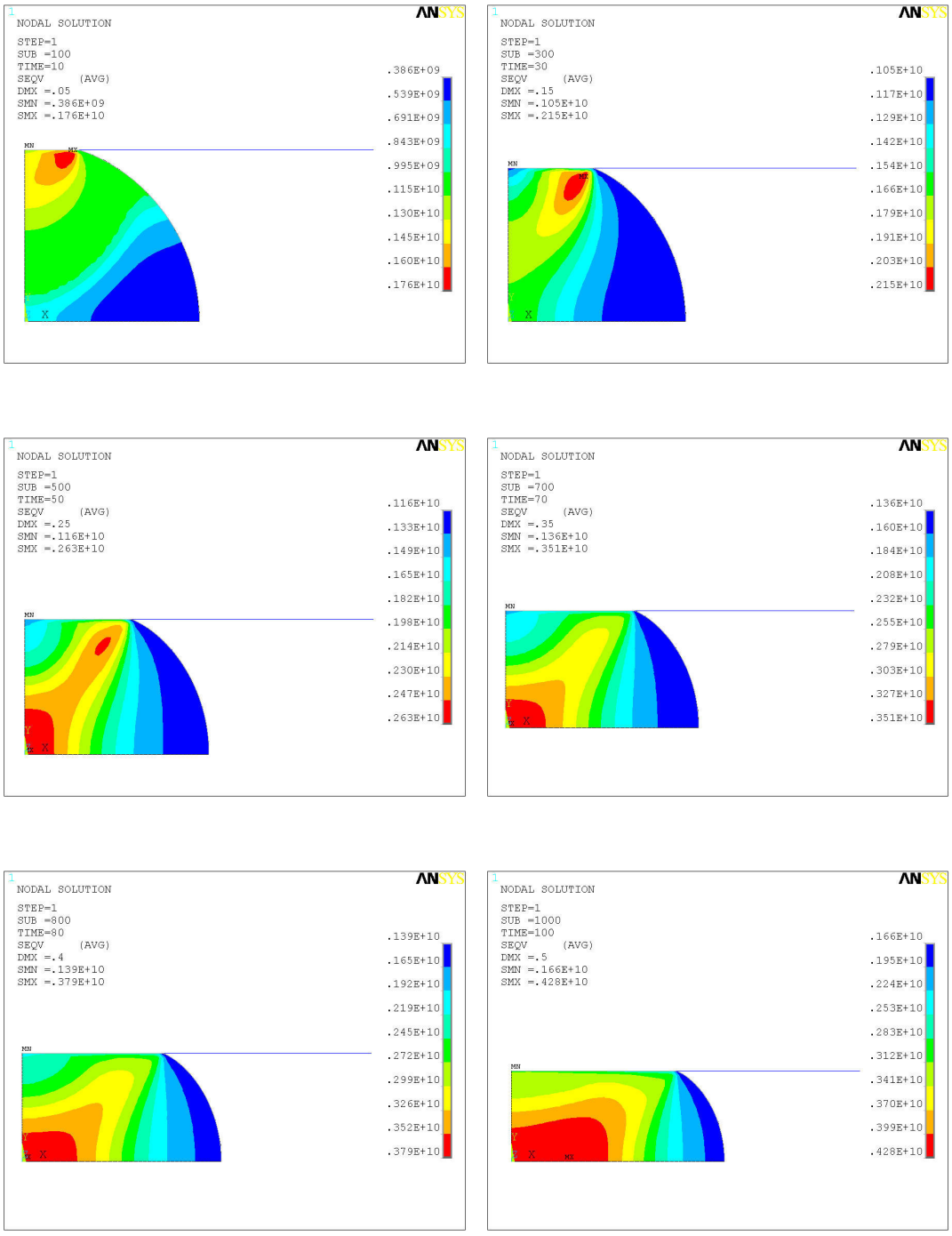

Figure 5.21: Von Mises stress distribution for 2% strain hardening in the sphere.

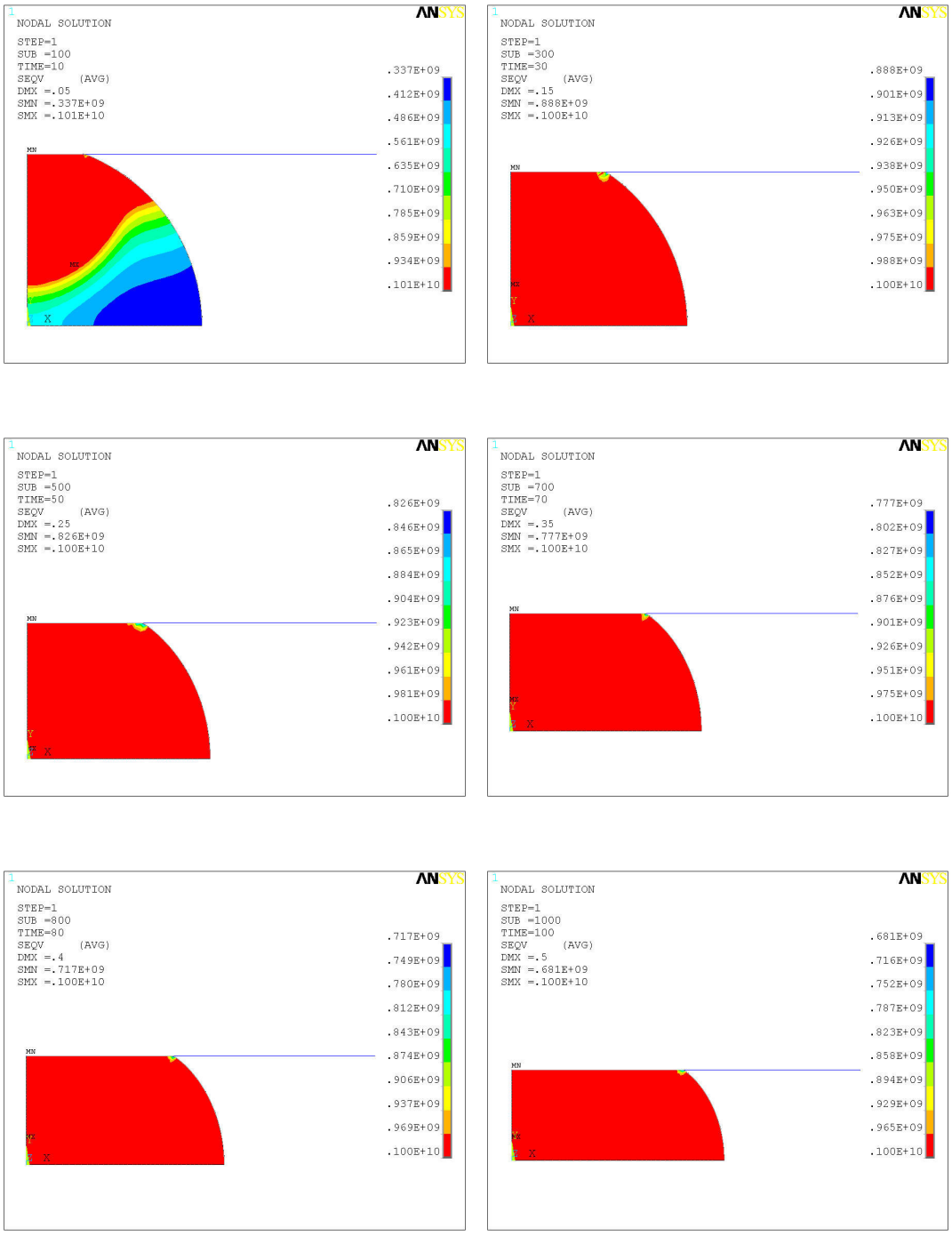

Figure. 5.22: Von Mises stress distribution for 0% strain hardening in the sphere.

5.3 The Effect of Friction

When a sphere is in contact with a flat rigid surface, in reality there will be some friction across the contact area. The study has not considered the effects of friction on the contact pressure and area until now. In this section an attempt is made to understand the effects of friction on the contact pressure and area. Friction is introduced in the contact area in the finite element modeling code by varying the coefficient of friction across the contact area.

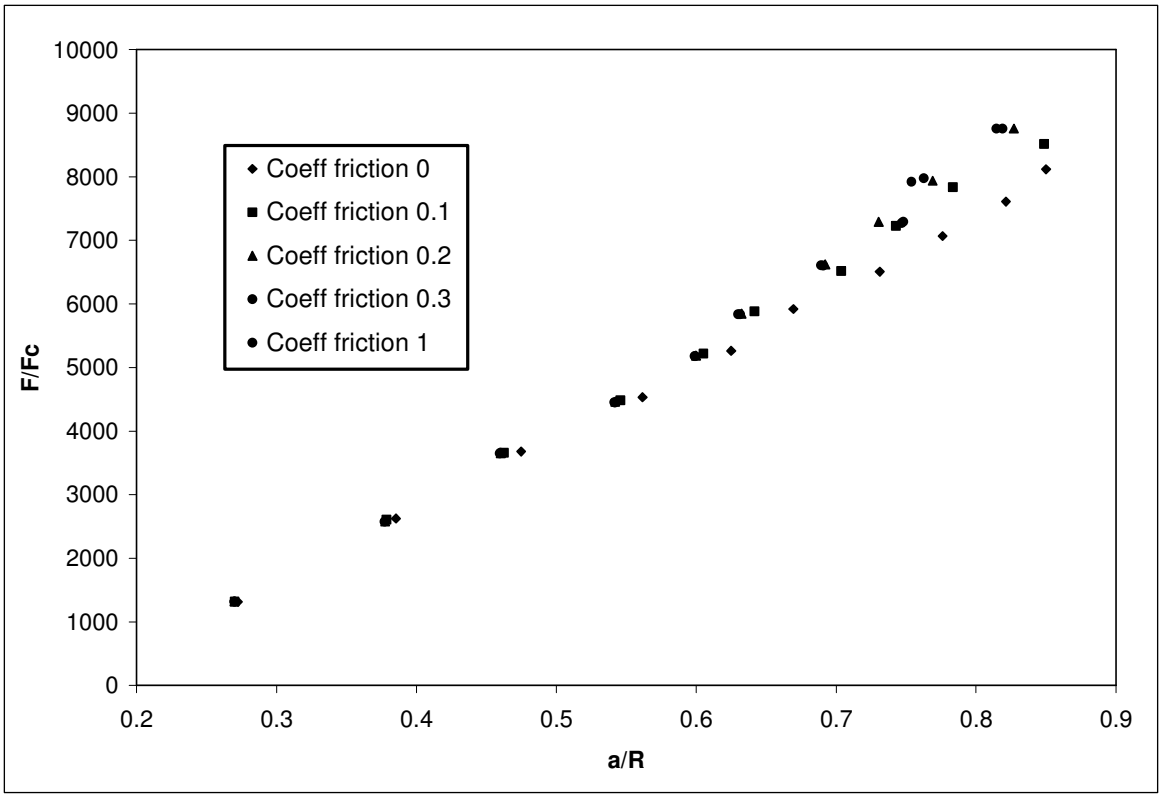

Figure 5.23: Variation of contact force with increasing contact radius

The results in Fig. (5.23) show that for increasing coefficients of friction across the contact area, the variation in contact force is not much for light loading however as the deformations get larger in Fig. (5.22), friction plays an important role in predicting the contact force. Comparisons with strain hardening results suggest that friction does not have a large effect relative to strain hardening. Also, increasing coefficients of friction affects the predictions in Fig. (5.23) only after $a/R = 0.5$. This suggests that friction does not play a major role until a/R becomes larger than 0.5.

It is important to understand whether strain hardening or friction has a greater effect on the contact force predictions. Figs. (5.24) and (5.25) show the effect of strain hardening and friction on the rigid base case predictions. It can be seen from the comparison that strain hardening starts affecting the predictions from small values contact radius *(a/R=0.2)* and friction plays a minor role compared to strain hardening and only affects the predictions for values of contact radius above 0.5. Hence friction plays a secondary role to strain hardening in predictions of contact force.

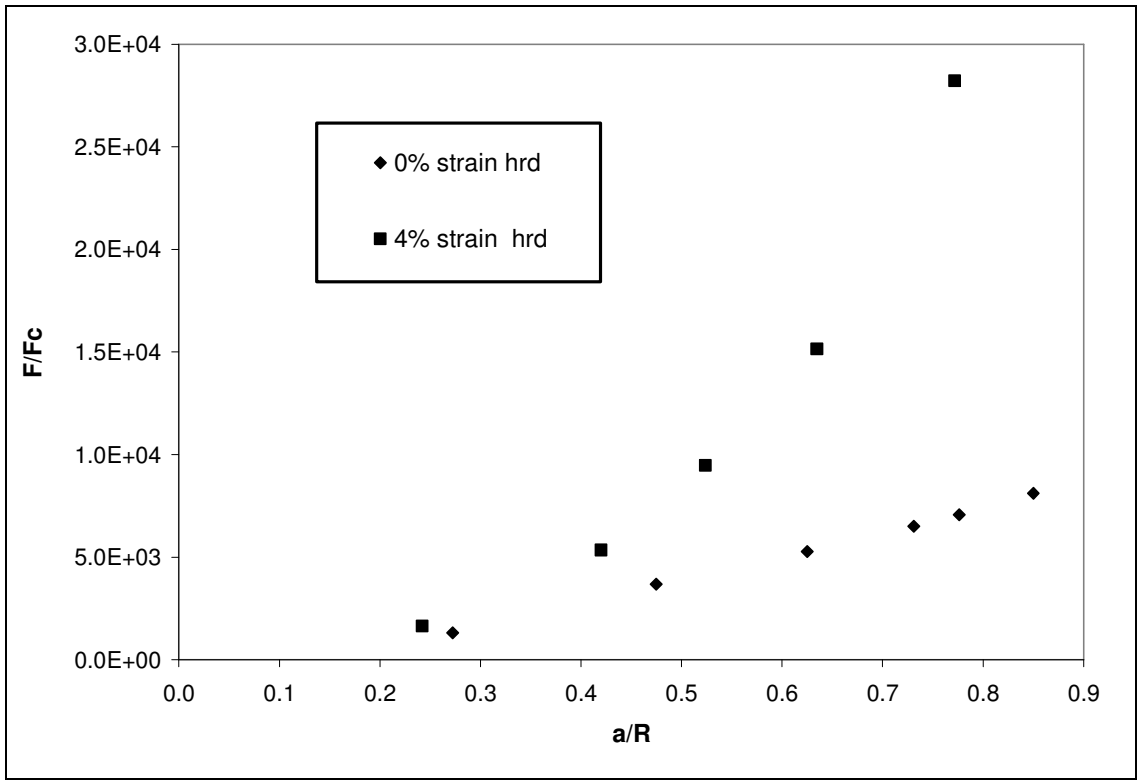

Figure 5.24: Effect of increasing strain hardening across the contact area on predictions of contact force

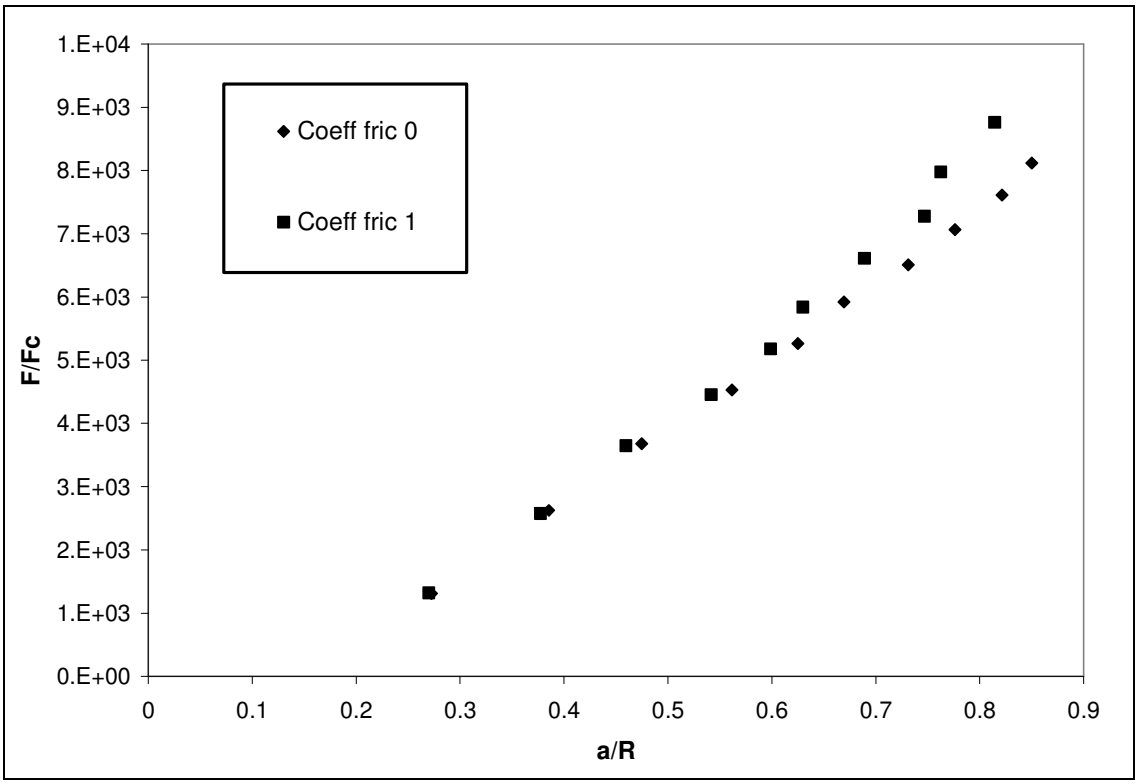

Figure 5.25: Effect of increasing friction across the contact area on predictions of contact force

CHAPTER 6

CONCLUSIONS

This work presents an FEM based model to predict the behavior of spherical surfaces being heavily compressed by flat rigid surfaces. In the initial part of the study, the material has been modeled as elastic-perfectly plastic to exclude strain hardening effects and friction across the contact area. Later the effects of strain hardening have also been studied. The model works well for both elasto-plastic deformations and for fully plastic deformations. Therefore a new model has been provided which can model a significantly larger range of deformation for spherical contacts. The model is based on the results of a FEM simulation of heavily loaded spherical contacts. The equations have been formulated using volume conservation theory and barreling theory for the compression of cylinders. Probably, the most important finding is that the effect of bulging or barreling must be considered in calculating a/R. The results show that when deformations are small, that the Jackson Green model may actually provide slightly more accurate results, but as deformations get larger the current model produces more accurate results in comparison to the FEM results.

The results of the finite element based model have also been verified with experimental data for different materials like brass and phosphor bronze provided by Chaudhri et al. [2]. The FEM based model compares surprisingly well with these

previous results, and without the use of any additional fitting parameters. There is some difference in the results because there is some hardening and friction occurring in the experimental measurements. The current study confirms the suggestions by Chaudhri [2] that barreling of cylinders has similarities in behavior to large deformations in spherical contact. Also, through various literature sources referred during current research, the constant in the relationship between contact pressure and yield strength (see Eq. (29)) seems have values ranging from 2.84 to 3.3. The current study found out that for phosphor bronze and brass the value that best replicated the experimental results is 3.15.

This work also studies the effect of strain hardening in spherical contact with severe deformation. Results of Von Mises stress distribution have been compared with Noyan [1] and similar patterns of hardening are found. Also, friction will play a secondary role in predictions of contact area and pressure. Some preliminary results have been shown to understand the variation of contact force with increasing contact area for various values of coefficient of friction. In the future the authors would like to further investigate these additional effects.

CHAPTER 7

RECOMMENDATIONS FOR FUTURE WORK

The current study presents the results of a FEM model and proposes a closed form equation for predicting contact pressure and area for spheres compressed under heavy loading. The results have been verified with real world experimental data and are in good agreement. The comparisons reveal that the results are in better agreement with phosphor bronze material than brass since this material (phosphor bronze) was work hardened before compression to have elastic perfectly plastic materials. In contrast, the brass spheres were not work hardened. In the simulations too, the spheres were modeled as elastic perfectly plastic. Hence the current model is more applicable to this case than actual spherical deformation in real applications.

An attempt was made to understand the effects of strain hardening and friction during compression of spheres. Preliminary results have been shown in the sections above. More work is needed to fully describe these effects. Fig. (5.19) reveals that friction will play a crucial role in predictions of contact force and pressure as the contact radius increases.

BIBLIOGRAPHY

1. Noyan, I C., *Plastic deformation of solid spheres.* Philosophical Magazine A, 1988. **57**(1): p. 127-141.
2. Chaudhri, M M., Hutchings, I M., and Makin P L, *Plastic Compression of Spheres.* Philosophical Magazine, 1984. **49**(4): p. 493-503.
3. Jackson, R L., Green, I., *A Finite Element Study of Elasto-Plastic Hemispherical Contact.* ASME J. Tribol., 2005. **127**(2): p. 343-354.
4. Jackson, R L. and Green, I., *A statistical model of elasto-plastic asperity contact between rough surfaces.* Tribology International, (2006). **39**: p. 906-914.
5. Chang, W R., Etsion, I., and Bogy, D B., *An Elastic-Plastic Model for the Contact of Rough Surfaces.* ASME J. Tribol., 1987. **109**(2): p. 257-263.
6. Liu, Z., Neville, A., *Analytical solution for elastic and elasti-plastic contact models.* Trib Trans, 200. **43(4)**: p. 627-34.
7. Mesarovic, S D., and Fleck, N A., *Frictionless Indentation of Dissimilar Elastic-plastic Spheres.* Int. J. Solids and Structures, 2000. **37**: p. 7071-7091.
8. Abbott, E J. and Firestone, F A., *Specifying Surface Quality-A Method Based on Accurate Measurement and Comparison.* Mech. Engr., 1933. **55**: p. 569-572.
9. Kogut, L. and Etsion, I., *Elastic-Plastic Contact Analysis of a Sphere and a Rigid Flat.* J. of Applied Mechanics, Trans. ASME, 2002. **69**(5): p. 657-662.
10. Zhao, Y., Maletta, D M., *An asperity microcontact model incorporating the transition from elastic deformation to fully plastic flow.* ASME J. Tribol, 2000(122): p. 86-93.
11. Jackson, R L., and Kogut, L., *A Comparison of Flattening and Indentation Approaches for Contact Mechanics Modeling of Single Asperity Contacts.* ASME J.of Tribology, 2005. **128**: p. 209-212.
12. Ye, N. and Komvopoulos, K., *Indentation analysis of elastic-plastic homogeneous and layered media: Criteria for determining the real material hardness.* Journal of Tribology, Trans. ASME, 2003. **125**(4): p. 685.
13. Jackson, R L. and Kogut, L., *Electrical Contact Resistance Theory for Anisotropic Conductive Films Considering Electron Tunneling and Particle Flattening.* IEEE Trans. on Components and Packaging Technologies, 2006. **30, No.1**.
14. Yim, M J. and Paik, K W., *Contact resistance and reliability of anisotropically conductive film (ACF).* IEEE Transactions on Advanced Packaging, 1999. **22**(2): p. 166-173.
15. Yin, C Y., *Experimental and modeling analysis of the reliability of the anisotropic conductive films*. 2003. New Orleans LA, United States: Institute of Electrical and Electronics Engineers Inc.
16. Avitzur, B., *Handbook of Metal-Forming Processes*. 1983, New York: Wiley.

17. Tabor, D., *The Hardness of Materials*. 1951, Oxford: Clarendon Press.
18. Greenwood, J A. and Tripp, J H., *The Contact of Two Nominally Flat Rough Surfaces.* Proc. Inst. Mech. Eng. 185, 1971: p. 625–633.
19. Nuri, K A. and Halling, J., *The normal approach between rough flat surfaces in contact.* Wear, 1975. **32**: p. 81-93.
20. Polycapou, A A. and Etsion, I., *Analytical approximations in modeling ocntacting rough surfaces.* ASME J. Tribol, 1999. **121(2)**(234-9).
21. Quicksall, J J., Jackson, R L. and Green, I., *Elasto Plastic hemispherical contact model for various mechanical properties.* IMechE. Journal of Eng. Tribology. Part. J. 218(4), 2004: p. 313-322.
22. Jackson, R L., Green, I. and Marghitu, D., *Predicting the Coefficient of Restitution of Impacting Elastic-Perfectly Plastic Spheres.* Nonlinear Dynamics, Accepted.
23. Megalingam, A. and Megalingam, M., *A FEM based Multiple Asperity Deterministic Contact Model.* Proceedings of ASME/STLE, 2009.
24. Shankar, S. and Mayuram, M M., *A Finite element based study on the elastic-plastic transition behavior in a hemisphere in contact with a rigid flat.* Journal of Tribology, Trans. ASME, 2008. **130**: p. 044502-1-044502-6.
25. Timoshenko, S., *Theory of Elasticity*. 1951, New York: McGraw-Hill.
26. Love, A E H., *A treatise on the mathematical theory of elasticity.* 1927.
27. Malayappan, S., Narayannasamy, R., and Kalidasamurugal, K., *A study of barreling behavior of aluminum billets during cold upsetting with an extrusion die constraint at one end.* Materials and Design, 2007. **28**: p. 954-961.
28. Narayanasamy, R., Sathiyarayanan, S., *A study on barrelling in magnesium alloy solid cylinders during cold upset forming.* Journal of Materials processing technology, 2000. **101**: p. 64-69.
29. Narayanasamy, R., *Phenomenon of barrelling in aluminium solid cylinders during cold upset forming.* Journal of Materials processing technology, 1997. **70**: p. 17-21.
30. Kulkarni, K M., *A study of barrelling as an example of free deformation.* ASME J. Eng. Ind, 1969. **91**: p. 743-754.
31. Ishlinksy, A J., *An English Translation has been published by Ministry of Supply,A.R.D. (1947).* Journal of Applied Math. Mech. (U.S.S.R), 1944. **8**: p. 233.
32. Johnson, K L., *Contact mechanics.* 1985.
33. Ashby, M., Johnson, K., *Materials:engineering, science, processing and design.* 2007.

APPENDIX

Finite element analysis Code

1. No Strain hardening considered –

```
/PREP7
CYL4,0,0,1,0,0,90
!*
ET,1,PLANE82
!*
KEYOPT,1,3,1
KEYOPT,1,5,0
KEYOPT,1,6,0
!*
!*
MPTEMP,,,,,,,,
MPTEMP,1,0
MPDATA,EX,1,,200E9
MPDATA,PRXY,1,,0.3
TBDE,BISO,1,,,
TB,BISO,1,1,2,
TBTEMP,0
TBDATA,,,2E9,,,,
APLOT
```

----------MESHING----------

```
SMRT,1
MSHAPE,0,2D
MSHKEY,0
!*
CM,_Y,AREA
ASEL, , , ,      1
CM,_Y1,AREA
CHKMSH,'AREA'
CMSEL,S,_Y
!*
AMESH,_Y1
```

```
!*
CMDELE,_Y
CMDELE,_Y1
CMDELE,_Y2
!*

K,5,2,1,0,
LSTR,      2,      5
!*
/REPLOT
!*
/COM,

------------------------------CONTACT PAIR CREATION - START ---------------------------

CM,_NODECM,NODE
CM,_ELEMCM,ELEM
CM,_KPCM,KP
CM,_LINECM,LINE
CM,_AREACM,AREA
CM,_VOLUCM,VOLU
/GSAV,CWZ,GSAV,,TEMP
MP,MU,1,0
MAT,1
MP,EMIS,1,7.88860905221E-031
R,3
REAL,3
ET,2,169
ET,3,172
R,3,,,1.0,0.1,0,
RMORE,,,1.0E20,0.0,1.0,
RMORE,0.0,0,1.0,,1.0,0.5
RMORE,0,1.0,1.0,0.0,,1.0
RMORE,10.0
KEYOPT,3,3,0
KEYOPT,3,4,2
KEYOPT,3,5,0
KEYOPT,3,7,0
KEYOPT,3,8,0
KEYOPT,3,9,0
KEYOPT,3,10,1
KEYOPT,3,11,0
KEYOPT,3,12,2
KEYOPT,3,2,3
KEYOPT,2,2,0
KEYOPT,2,3,0
```

```
--------------------------------GENERATE THE TARGET SURFACE  ------------------------

LSEL,S,,,4
CM,_TARGET,LINE
TYPE,2
LATT,-1,3,2,-1
TYPE,2
LMESH,ALL

-----------------------------GENERATE THE CONTACT SURFACE  -------------------------

LSEL,S,,,1
CM,_CONTACT,LINE
TYPE,3
NSLL,S,1
ESLN,S,0
ESURF
*SET,_REALID,3
ALLSEL
ESEL,ALL
ESEL,S,TYPE,,2
ESEL,A,TYPE,,3
ESEL,R,REAL,,3
LSEL,S,REAL,,3
/PSYMB,ESYS,1
/PNUM,TYPE,1
/NUM,1
EPLOT
ESEL,ALL
ESEL,S,TYPE,,2
ESEL,A,TYPE,,3
ESEL,R,REAL,,3
LSEL,S,REAL,,3
CMSEL,A,_NODECM
CMDEL,_NODECM
CMSEL,A,_ELEMCM
CMDEL,_ELEMCM
CMSEL,S,_KPCM
CMDEL,_KPCM
CMSEL,S,_LINECM
CMDEL,_LINECM
CMSEL,S,_AREACM
CMDEL,_AREACM
CMSEL,S,_VOLUCM
CMDEL,_VOLUCM
```

```
/GRES,CWZ,GSAV
CMDEL,_TARGET
CMDEL,_CONTACT
/COM,
----------------------------------CONTACT PAIR CREATION - END   --------------------------

/MREP,EPLOT
/REPLOT
FINISH
/SOL
FINISH
/PREP7
FINISH
/SOL
FINISH
/PREP7
FINISH
/SOL
FINISH
/PREP7
FINISH
/SOL

-------------------------------------BOUNDARY CONDITIONS ------------------------------

FLST,2,79,1,ORDE,4
FITEM,2,1
FITEM,2,3
FITEM,2,204
FITEM,2,-280
!*
/GO
D,P51X, , , , , ,UY, , , , ,
FLST,2,79,1,ORDE,4
FITEM,2,2
FITEM,2,-3
FITEM,2,127
FITEM,2,-203
!*
/GO
D,P51X, ,0, , , ,UX, , , , ,
FLST,2,1,4,ORDE,1
FITEM,2,4
!*
/GO
DL,P51X, ,UY,-0.5
```

----------ANALYSIS TYPE----------

```
ANTYPE,0
NLGEOM,1
DELTIM,0.1,0,0
AUTOTS,0
TIME,100
OUTRES,ALL,-10
/STATUS,SOLU
```

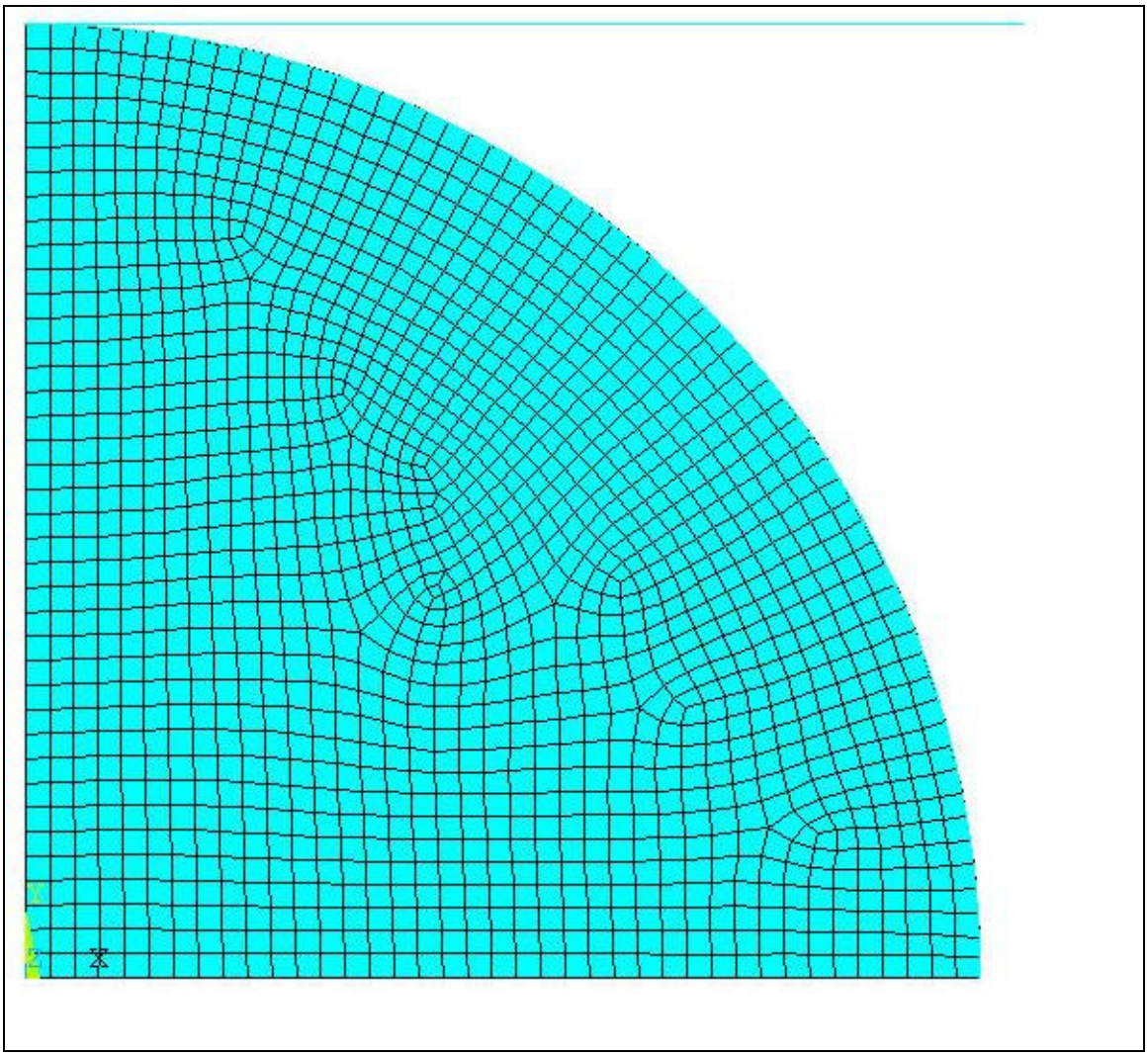

Figure A.1: Undeformed sphere with FEA mesh